Ablation of VEGFA following a lumbar intervertebral disc injury attenuates intradiscal neurovascular features and prevents chronic low back pain symptoms

Authors: *Ryan S. Potter[1,2], *Hong J. Moon[2], *Sade W. Clayton[2], Remy E. Walk[3], Addison L. Liefer[3], Liufang Jing[3], Amber N. Stratman[4], Lori A. Setton[1,2,3], Munish C. Gupta[2], Simon Y. Tang[1,2,3]
***These authors led the study equally.**

Affiliations:

[1] Department of Mechanical Engineering and Materials Science, Washington University in St. Louis
[2] Department of Orthopaedic Surgery, Washington University School of Medicine
[3] Department of Biomedical Engineering, Washington University in St. Louis
[4] Department of Cell Biology and Physiology, Washington University School of Medicine

Corresponding author: Simon Tang (simon.tang@wustl.edu)

One Sentence Summary:
VEGFA critically mediates the infiltration of neurovascular features into the degenerating intervertebral disc and subsequent low back pain symptoms, and the ablation of VEGFA prevents chronic low back pain behavior.

Keywords:
VEGFA, intervertebral disc injury, low back pain, neurovascular features, preclinical model

Abstract

There are currently no therapies for the staggering disability and public health costs of chronic low back pain (LBP). Innervation of the degenerating intervertebral disc (IVD) is suspected to cause discogenic LBP, but the mechanisms that orchestrate the IVD's neo-innervation and subsequent symptoms of LBP remain unknown. We hypothesize that Vascular Endothelial Growth Factor-A (VEGFA) critically mediates the neurite invasion in the IVD and contributes to prolonged LBP. Initiating IVD degeneration through a mechanical injury, we evaluated the progression of neurovascular features into the IVD, as well as resultant LBP symptoms and locomotive performance at acute (3-weeks) and prolonged (12-weeks) time points following the IVD injury. To determine the role of VEGFA, we used a mouse model with ubiquitously inducible recombination of the floxed Vegfa allele (UBC-Cre^{ERT2}; *Vegfa*$^{fl/fl}$). The ablation of VEGFA attenuated the neurite and vessel infiltration into the degenerating IVD, and the VEGFA-null animals exhibited alleviated mechanical allodynia and improved locomotive performance. To determine the effects of IVD-derived VEGFA on endothelial cells and neurons, we cultured HMEC-1 endothelial cells and SH-SY5Y neurons using conditioned media from *VEGFA*-silenced (siRNA) human primary IVD cells stimulated by IL1β. The endothelial cells and neurons exposed to the secretome of the *VEGFA*-silenced IVD cells exhibited reduced growth, suggesting that the inhibition of IVD-derived VEGFA may be sufficient to attenuate intradiscal neurovascular features. Together, we show that VEGFA orchestrates the growth of intradiscal vessels and neurites that cause low back pain and impaired function, and the inhibition of VEGFA prevents prolonged sensitivity and motor impairment associated with discogenic low back pain.

INTRODUCTION

Low back pain (LBP) is a prevalent, debilitating, costly, and multifactorial condition worldwide, imposing substantial global and economic burdens [1-3]. LBP affects as much as 80% of the population, and the elderly experience greater rates of LBP that exacerbate their functional decline, frailty, and loss of independence [4]. LBP is the leading cause of years lived with disability and contributes an estimated $50 to $100 billion USD annually in healthcare costs [4-6]. Chronic LBP is commonly associated with intervertebral disc (IVD) degeneration, which occurs with aging, genetic predisposition, and injury [7-10]. Degeneration leads to structural and biochemical changes in the IVD, including the loss of hydration, inflammation, and matrix breakdown [11-14]. Despite our understanding of the features of IVD degeneration, it remains unclear which specific features of degeneration are mechanistically responsible for the eventual low back pain [15]. While the healthy IVD is relatively aneural, the painful human intervertebral discs are innervated, suggesting a role for aberrant nerve growth in discogenic pain [16]. VEGFA (Vascular Endothelial Growth Factor A) is a potent signaling protein that promotes the proliferation, migration, and survival of endothelial and neural cells[17-19]. While VEGFA has known roles in both vascular and neural support, its function following an IVD injury, and how it initiates or sustains discogenic pain remain unresolved. We hypothesized that VEGFA is crucial for the neurite growth and vascularization in the injured IVD to mediate acute and chronic discogenic pain.

To investigate the role of VEGFA in IVD degeneration and low back pain, we utilized a mouse model with an inducible global ablation of VEGFA. To model discogenic low back pain, we created an injury in the lumbar IVD to initiate degeneration [20-22]. We subsequently measured pain-related symptoms such as mechanical and thermal sensitivity as well as locomotor function [20]. Because VEGFA is also a critical regulator of vascular growth, we assessed neo-vascularization into the injured IVD along with neural

71 infiltration to better understand the relationship between vascular and neural response in disc
72 degeneration. To evaluate whether there was peripheral nervous system adaptation, we evaluated pain-
73 related ion channels expression in the lumbar dorsal root ganglions (DRGs). To determine the role of
74 IVD-produced VEGFA on neuron and endothelial cell growth we performed co-culture experiments
75 using human cells.
76
77 Our findings show that VEGFA plays a central role in promoting neurovascular ingrowth into the
78 degenerating intervertebral disc contributing to chronic low back pain. The ablation of VEGFA reduced
79 neurite and blood vessel infiltration into the injured disc and alleviated mechanical allodynia and
80 locomotor deficits in mice. VEGFA ablation also attenuated pain-related ion-channel expression in the
81 DRGs of the injured animals. In vitro, endothelial cells and neurons exposed to conditioned media from
82 VEGFA-silenced IVD cells exhibited diminished growth, reinforcing VEGFA's role as a key mediator
83 of vascular and neurite infiltration. These results demonstrate that targeted inhibition of VEGFA can
84 suppress intradiscal vessels and neurites that cause low back pain and impaired function.

RESULTS

Removal of VEGFA Blunts Intradiscal Invasion of Neurovascular Structures

In WT animals, the injured IVD was infiltrated by PGP9.5+ neurons and by endomucin+ vessels. VEGFA ablation significantly blunted these neuronal and vascular features. Immunofluorescence images from 50µm thick sections (Figure 1A-B) showed fewer neural and vascular structures in VEGFA-null mice compared to WT particularly in the region around the outer annulus fibrosus (AF) near the injury site. Quantitative measurements of structural length and depth (Figure 1C-F) revealed diminished neurite length (p=0.01), vessel length (p=0.004), neurite depth (p=0.002), and vessel depth (p=0.047) due to VEGFA removal. Post hoc analysis reveals differences between the WT and VEGFA-null IVDs in neurite depth at 3 weeks (p=0.001) and in vessel length at 12 weeks (p=0.01). These findings show that VEGFA is crucial for instigating the neural and vascular structures in IVDs following injury. VEGFA ablation also limited the penetration into- and the propagation within- of these structures of the IVD. No sex-differences in nerve or vessel growth were observed (Table S1).

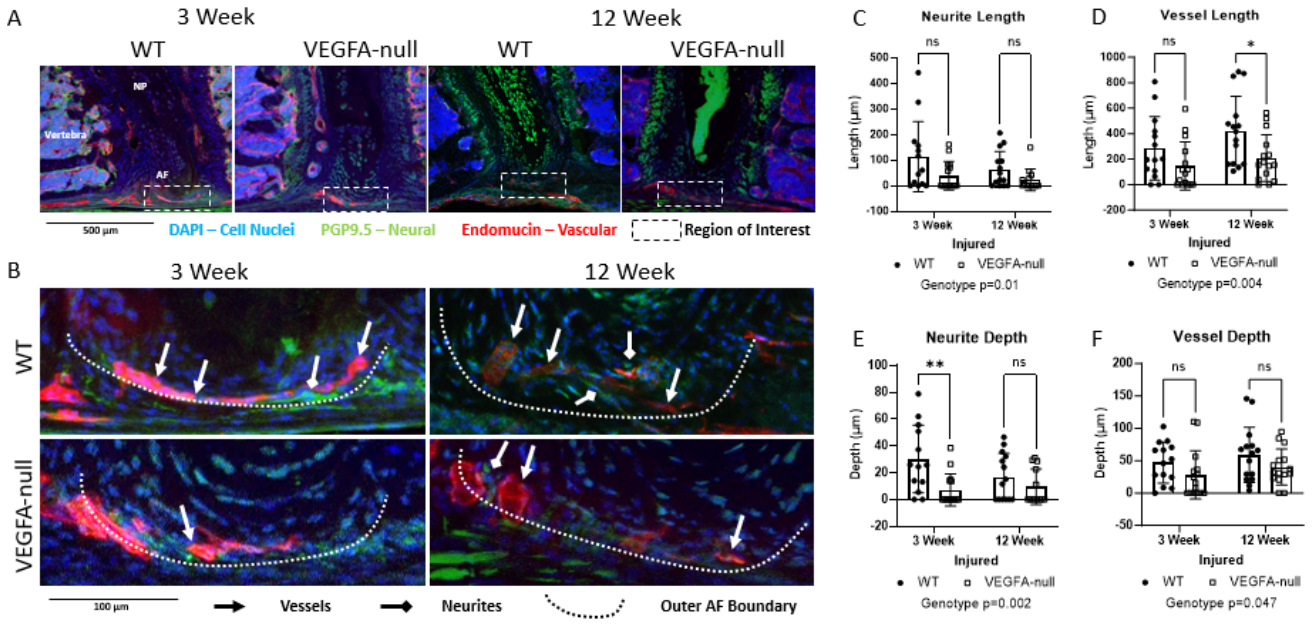

Fig. 1: Removal of VEGFA Blunts Intradiscal Invasion of Neurovascular Structures Following IVD Injury. A) IHC of dorsal sides of the injured lumbar IVD with the nuclei (DAPI) in blue, neuronal features (PGP9.5) in green and vascular features (Endomucin) in red. The region-of-interest (ROI) is boxed with dotted lines. B) Outer AF ROI with key features notated C-F) VEGFA loss reduces neurite lengths (p=0.01) and vessel lengths (p=0.004) across both post-injury time points. Likewise, the neurite penetration depth (p=0.002) and vessel penetration depth (p=0.047) are blunted by VEGFA removal. Data are presented as mean ± standard deviation.

VEGFA Is Essential for the Spatial Colocalization of Intradiscal Nerves and Vessels

The spatial proximity of intradiscal nerves and vessels are disrupted by VEGFA ablation. Immunofluorescence images reveal the distribution of neural (PGP9.5, green) and vascular (Endomucin, red) structures highlighting the regions of interest around the outer annulus fibrosus (AF) and overlapping lengths relative to neurites (Figure 2A-B). The colocalization analysis show that the WT injured IVDs have neurites with a large amount of vessels in their proximity. The removal of VEGFA in the IVDs 3 weeks following injury protected a higher number of IVDs from infiltrating neurites (Figure 2-C), but there was no difference in the number of IVDs with de novo neurites between the VEGFA-null and WT animals at 12 weeks after injury. The loss of VEGFA did not deter Endomucin+ vessels from penetrating the injured IVD at both time points (Figure 2D). The spatial overlap analysis between neurites and vessels (Figure 2E) show that VEGFA ablation dramatically reduces the amount of neurites near vessels (p=0.007). After adjusting for the length of the neurites, this observation remains robust independent of the basal level of neurites in each animal (p=0.008; Figure 2F). The lack of difference over time between the depth and the length ratios between the neurites and vessels indicates that once initiated, VEGFA does not appear to affect the propagation of these features (Figure 2G-H).

These findings highlight the critical role of VEGFA in the initiation of neural and vascular features in the IVD.

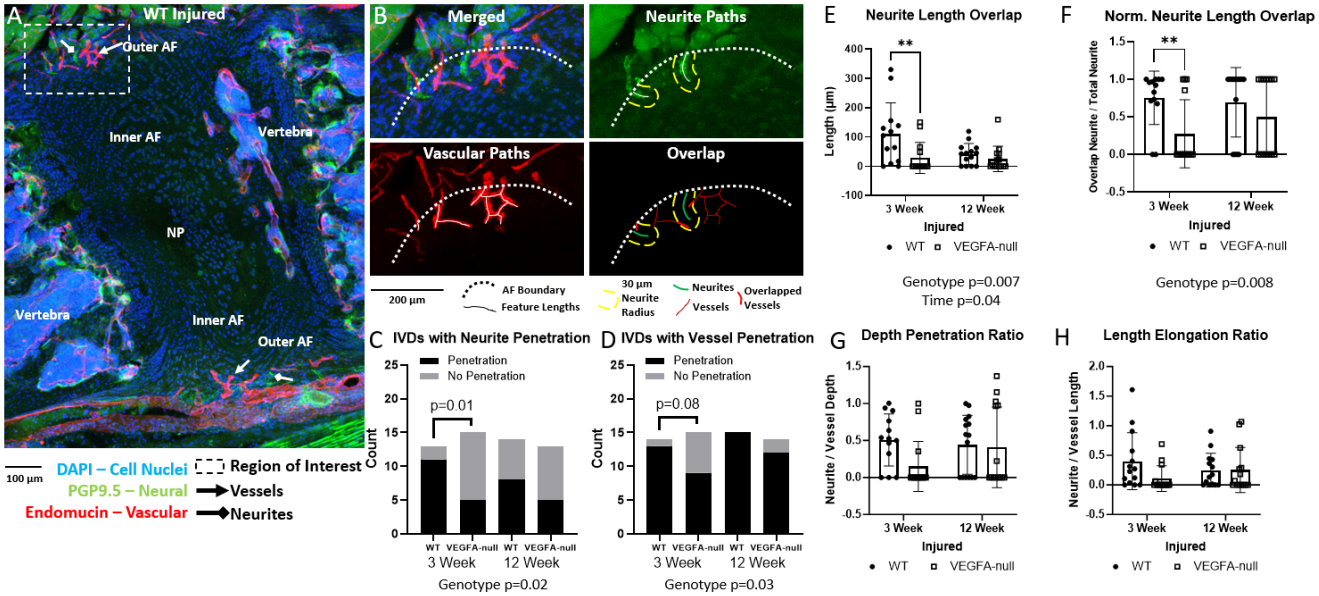

Fig. 2: VEGFA is Essential for the Colocalization of Intradiscal Nerves and Vessels Initiation. A) WT injured disc showing key features of the IVD and a ROI for analysis B) Graphical representation of how spatial colocalization analyses quantified the number of neurites that were in proximity of vessels within a 30 µm region. C-D) Loss of VEGFA significantly reduced the number of injured IVDs that experienced infiltrating neurites 3 weeks after injury (p=0.01) in VEGFA-null. Neurite (p=0.02) and vessel (p=0.03) infiltration both show a significant decrease in VEGFA-null groups. E) VEGFA ablation reduced the amount of vessel-adjacent neurites (p=0.007). F) The effect of VEGFA loss on preventing neurite-vessel spatial coupling persevered even when accounting for varying intradiscal neurite lengths between different animals (p=0.008), confirming that this local phenomenon is conserved across animals. G-H) The lack of difference in the depth penetration and length elongation ratios suggest that, on average, once the neurites have initiated, the loss of VEGFA does not appear to affect their propagation. Statistical model C-D: Fisher's exact test. Statistical model E-H: 2 factor ANOVA with Fisher LSD post-hoc comparisons. E-H Data are presented as mean ± standard deviation.

Depletion of VEGFA Suppresses the Expression of Pain-related Ion Channels in the DRG

Quantitative measurements of corrected total cell fluorescence (CTCF) of mouse lumbar (left, L3-L6) dorsal root ganglia (DRGs; Figure 3B-D) revealed a significant reduction in transient receptor potential ankyrin 1 (TRPA1) fluorescence (p=0.04) due to VEGFA removal following injury. No significant changes were measured in tyrosine kinase receptor A (TrKA) or transient receptor potential vanilloid 1 (TRPV1) CTCF levels due to the loss of VEGFA ablation.

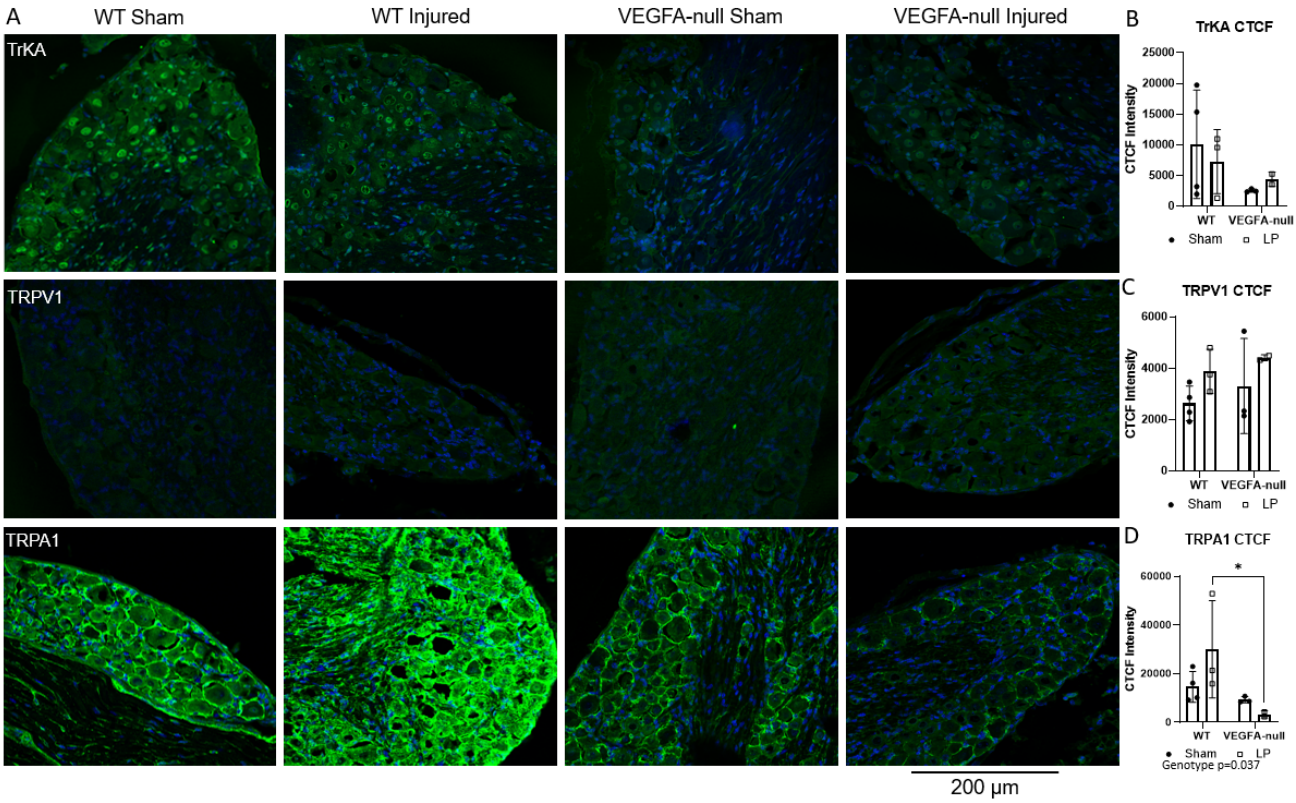

Fig. 3: VEGFA Inhibition Reduces the Expression of Pain-related Ion Channels in the DRG. A) TrKA (top), TRPV1 (middle), and TRPA1 (bottom) in green and DAPI in blue were quantified. B-D) Corrected total cell fluorescence (CTCF) for each sensory ion channel shows VEGFA ablation regulated TRPA1 expression (p=0.037).

50 **Ablation of VEGFA Alleviates Mechanical Sensitivity and Locomotive Function**

51 *Loss of VEGFA Attenuates Mechanical, but Not Hot or Cold, Sensitivity*

52 WT animals exhibited mechanical sensitivity measured by the Von Frey filament test at both 3 and 12
53 weeks after the IVD injury. Ablation of VEGFA partially restored this impairment at the 12-week time
54 point (p=0.001, Figure 4A), although no effects of VEGFA ablation was observed at 3-weeks following
55 IVD injury. The electronic Von Frey filament test also revealed that there is a greater mechanical
56 sensitivity on the left side of the surgical approach. VEGFA removal specifically alleviated the
57 mechanical sensitivity of the injured side, without modifying the contralateral side (Figure S1F). No
58 notable changes were observed in heat or cold sensitivity at any post-operative time point (Figure 4B-
59 C; Table S1).

60 *VEGFA Ablation Improves Rotarod Performance, but Does Not Affect Passive Function*

61 We also evaluated locomotive performance through an active challenge of locomotive function,
62 measured through the rotarod assay, longitudinally, every three weeks up to 12 weeks after injury. The
63 longitudinal rotarod test (Figure 4D) reveals that VEGFA-null mice exhibited longer latencies to fall at
64 9- and 12-weeks post-injury compared to impaired WT (p=0.004), highlighting progressive motor
65 coordination decline over time in the WT animals (p=0.003). In the Open Field test, total distance
66 traveled (Figure 4E) and rearing counts (Figure 4F) were not different between genotypes, sex,
67 tamoxifen, or due to surgery (Table S1), suggesting comparable levels of exploratory behavior and
68 general activity between all groups.

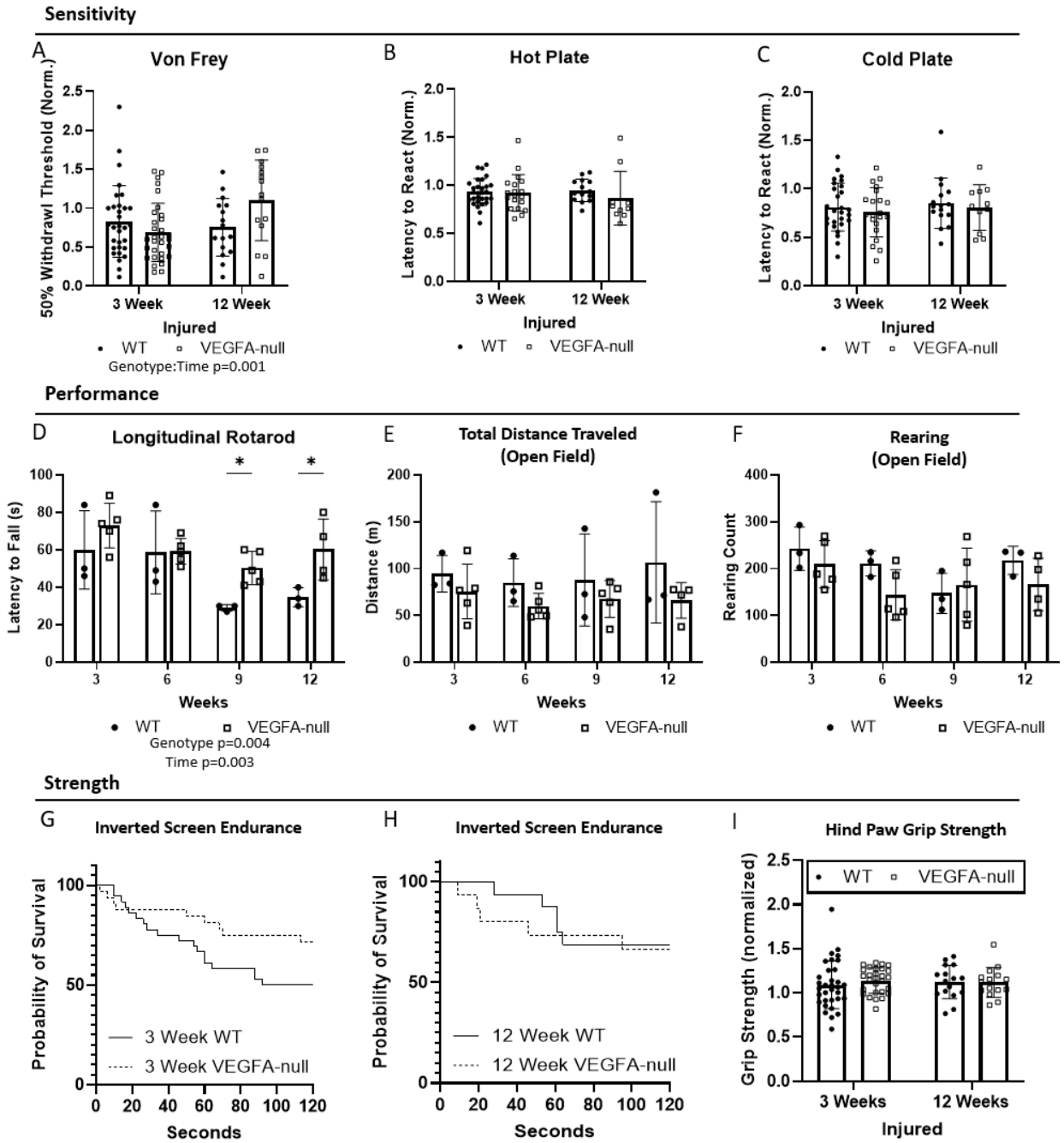

Fig. 4: VEGFA Ablation Improves Mechanical Sensitivity and Performance A) Mechanical sensitivity shows a significant interaction between genotype and time (p=0.001) in mice following IVD injury with a worsening effect seen in WT leading to a chronic sensitivity and an improving effect in VEGFA-null over time. B-C) No evidence of differences in hot or cold sensitivity was observed at any

time. D) There was evidence of significant differences in longitudinal measures of performance that included rotarod (genotype, p=0.004; time, p=0.003), indicative of a VEGFA rescue of an injury associated progression of decreased performance in the rotarod test. E-F) There was no evidence of differences in any measures of open field with genotype and at any time point. G-I) There was no evidence of differences in inverted screen endurance or hind paw grip strength with genotype and at any time point. Statistical model A-F, I: Linear mixed effects with genotype and time as factors with post-hoc LSM with Sidak correction. G-H Mantel-Cox test. A-F, I Data are presented as mean ± standard deviation.

Assay	Sex M/F	Tamoxifen +/-	Naïve/Sham
Von Frey	0.94	0.63	0.66
Grip Strength	0.09	0.92	0.07
Inverted Screen	0.65	0.33	0.64
Cold Sensitivity	0.52	0.06	0.40
Heat Sensitivity	0.44	0.47	0.57
Rotarod	0.34	0.43	0.25
Distance (Open Field)	0.33	0.27	0.18
Rearing (Open Field)	0.25	0.32	0.59
Neurite Length	0.08	NA	NA
Vessel Length	0.19	NA	NA
Neurite Depth	0.51	NA	NA
Vessel Depth	0.15	NA	NA

Table S1: Behavioral and Neurovascular Comparisons for Sex, Tamoxifen, and Naïve/Sham. Assays that were not found to produce evidence of differences between genotypes and at any time point following IVD injury. The respective p-values are shown for comparisons between Male and Female, Tamoxifen +/-, and Naïve and Sham surgery for the behavioral, neuronal, and vascular assays. P-values are obtained from the Linear Mixed Effects statistical model. Factors not relevant for comparison are shown as NA.

87

88 *VEGFA Removal Does Not Affect Measures of Strength*

89 To determine overall impacts on much function following VEGFA ablation, strength assessments were
90 conducted, including inverted screen endurance and hind paw grip strength analysis. The inverted screen
91 endurance test, presented using Kaplan-Meier curves, showed that VEGFA-null mice have similar
92 probabilities of hanging on the wired mesh compared to WT at both 3 weeks (Figure 4G) and 12 weeks
93 (Figure 4H). Measures of hind paw grip strength (Figure 4I) were also found to be similar across
94 genotypes, indicating no compromise in muscle function from VEGFA ablation.

95 Overall, the behavioral and locomotive function analyses show that VEGFA-null mice have
96 improved recovery of mechanical sensitivity and avert the transition to chronic sensitivity seen in the
97 WT while also avoiding the performance deficits in WT at chronic time points. However

98

99 **Ablation of VEGFA does not affect structure, function, or degeneration of the IVD**

00 *Loss of VEGFA Does Not Affect the Histopathologic Degeneration of the IVD*

01 CEμCT analysis of the IVDs 3 weeks after injury reveals significant deterioration of the IVD structure.
02 By using a contrast enhancing agent, Ioversol, the injury was observed on the ventral side of the outer
03 AF as progressively higher attenuating regions that mark the fibrous scar tissues (Figure 5A). The
04 injured IVDs also exhibit a loss of NP attenuation, measured by NI/DI, demonstrating the loss of the
05 water retaining ability of the NP ($p=0.03$, Figure 5B). The ablation of VEGFA does not affect these
06 injury-mediated changes in degeneration. A narrowing of the intradiscal space measured by disc height
07 index (DHI), a hallmark of IVD degeneration, is apparent in all of the injured discs ($p=0.01$, Figure 5C)
08 with no evidence of differences among genotypes or with post-operative time. Surprisingly, there was

09 not a change in NP volume either due to injury or VEGFA ablation (Figure 5D). Injury increases the
10 degenerate features including decreased NP hydration and a narrowing DHI; VEGFA ablation did not
11 appear to alleviate these tissue-level changes in the IVD.

12 *Injury to the IVD Does Not Impair Its Mechanical Function*

13 Dynamic compression of IVDs 3 weeks post injury show no distinct mechanical responses to injury or
14 impact from VEGFA ablation. The stiffness measurements show no significant differences between WT
15 and VEGFA-null groups, both in sham and injured conditions (Figure 5E). Likewise, the dissipation
16 factor indicates a similar response with no appreciable changes from injury or VEGFA loss (Figure 5F).
17 These findings show that the degeneration that occurs at 3 weeks after injury in this model does not yet
18 impair the IVD's mechanical function.

19 *VEGFA Loss Does Not Rescue the Degenerative Changes Caused by Injury*

20 Histopathological scoring (Figure 5G-H) revealed the damaging effects of a needle stab on the
21 compartments in the disc, including decreased NP cell density and changes in cellular morphology,
22 disruption of the AF concentric lamellar structures with increased cellularity and presence of clefts,
23 along with thinning and disruptions in the endplate cartilage, and structural disorganization in the
24 boundary regions. Scores for injured groups averaged near 26 out of a 36 possible for maximal injury,
25 while sham controls averaged 11 ($p < 0.0001$). Statistical differences due to VEGFA removal were not
26 detected. IVD injury dramatically changed all compartments of the disc with the largest effects on the
27 AF followed by NP while sham scores indicate mild degeneration from the surgical exposure of the disc
28 and likely disruption of surrounding soft tissues.

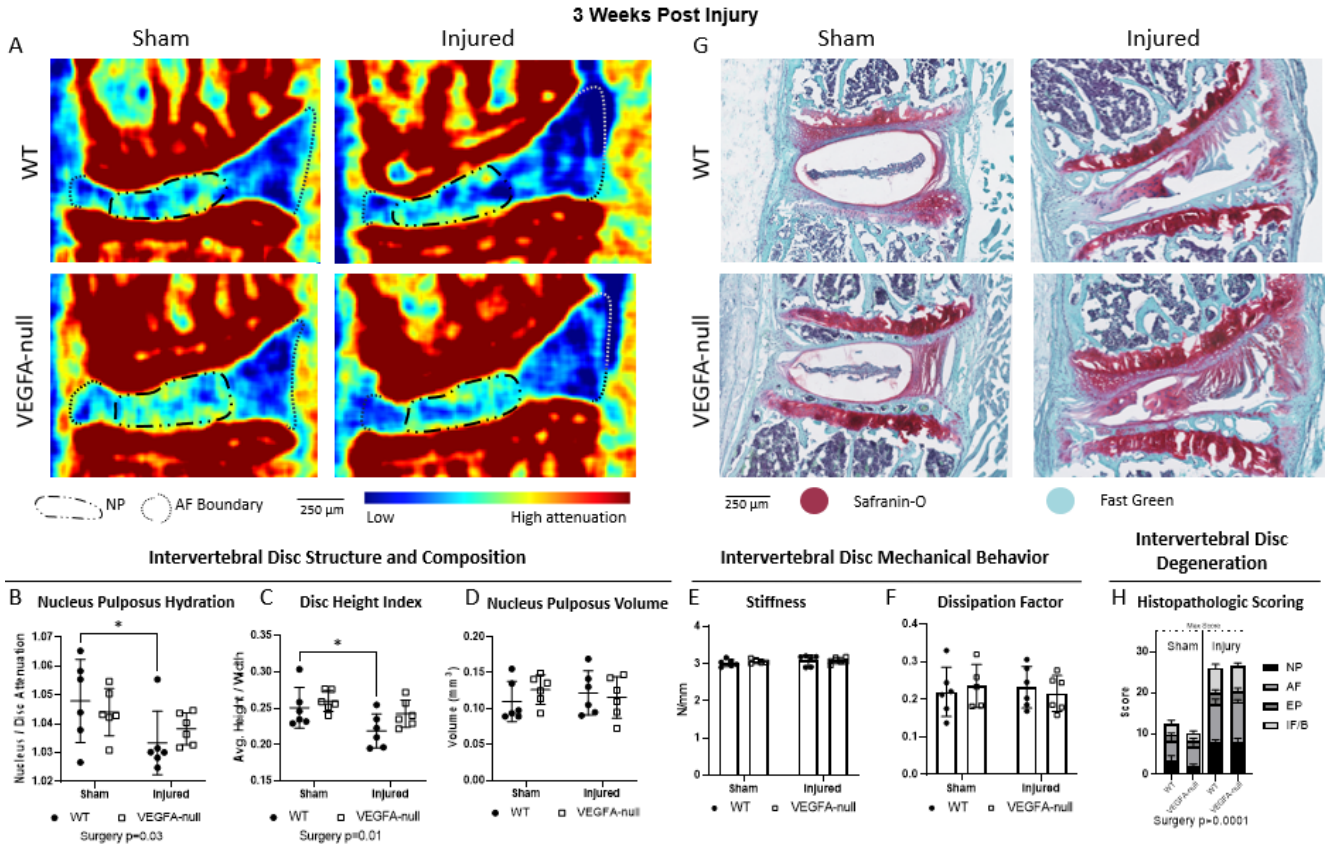

Fig. 5: Loss of VEGFA Does Not Alter Structural, Mechanical, or Histopathologic Degeneration to the Injured IVD. A) IVD structure analyses via CEµCT show that B) injury decreased NP hydration (p=0.03), indicated by the decreased attenuation of the NP compared to sham. C) injury decreased disc height index, DHI, (*, p=0.01) compared to sham, and D) no effect of injury was observed on NP volume. Changes to mechanical behavior were not observed in E) stiffness and F) dissipation factor, indicating that tissue level mechanics were not changed by injury or VEGFA removal at 3-weeks post injury. G) Histological images stained with Safranin-O and Fast Green show IVD degeneration. H) Histopathologic scoring shows a strong effect of injury (*, p<0.0001) with no appreciable differences due to VEGFA loss in nucleus pulposus, annulus fibrosus, end plate, or the interface/boundary demonstrating the pathophysiological response from needle puncture. Data are presented as mean ± standard deviation.

41 **Silencing *VEGFA* RNA in Human IVD Cells Attenuates the Growth of Co-Cultured Neuronal and**
42 **Endothelial Cells**

43 Transfecting human IVD cells with VEGFA-specific small interfering RNA (siRNA) suppressed their
44 production of the VEGFA protein production by 57.4% when stimulated with IL-1β (Figure S6).
45 Coculturing these VEGFA-siRNA transfected, IL-1β stimulated IVD cells with SH-SY5Y neurons
46 maintained the neuron morphology but blunted the growth of the axonal extensions (Figure 6A).
47 Although there was no difference in the number of neurites and their averaged lengths for co-cultured
48 neurons (Figure 6B-C), the total neurite length, which is a product of these two measurements, reveals
49 a decrease in neurite growth co-cultured with VEGFA-siRNA transfected IVD cells (Figure 6D). RNA
50 sequencing revealed that neurons cultured with VEGFA-knockdown IVD cells expressed 39
51 downregulated and 107 upregulated differentially expressed genes (DEGs) when compared to those
52 neurons cultured with VEGFA-intact IVD cells (Figure 6E). Gene ontology analysis determined the
53 most enriched biological process from the DEGs involved the regulation of general cell processes, e.g.
54 GPCR signaling pathway, known for neurovascular development (*EDNRA, CHGA, RAMP3*), regulation
55 of growth (*DCC, GREM1, STC2, MYOZ1, MT1F, BST2, IGFBP3, CXCR4, MT1X, IGFBP7, BCL2*), and
56 the negative regulation of cell population proliferation (*GREM1, PTPN14, DHRS2, SSTR2, SCG2,*
57 *SERPINF1, IGFBP3, OVOL1, ADM, IGFBP7, BCL2, S100A11*). Notably, several DEGs were specific
58 to cell growth inhibition (*SSTR2, S100A11),* immune cells and inflammation (*CXCR4, FGFB2, IL32)*,
59 and neuronal cell functions (*DCC, SDK2*, *ASTN2*).
60

61 We also co-cultured VEGFA-siRNA transfected IVD cells, first stimulated with IL-1β, with the HMEC-
62 1 endothelial cells (aka ECs). The ECs cocultured with VEGFA-silenced human IVD cells were less
63 capable of forming closed tubes, a measure of angiogenesis (Figure 7A). ECs cultured with Scram

siRNA developed a higher number of closed loops than ECs cultured with VEGFA-siRNA (p=0.04) after 6 hours of culturing. (Figure 7B). RNAseq uncovered 175 downregulated and 0 upregulated DEGs when ECs are cultured with IVD cells transfected with Scram versus VEGFA siRNA (Figure 7C). Gene ontology analysis determined the most enriched biological processes from the DEGs were involved in vessel and vasculature related processes, These included lymph vessel development (*NR2F2, TBX1, SOX18, EFNB2, HEG1*), blood vessel morphogenesis (*TNFAIP2, EFNB2, HEG1, PRKACA, NRARP, TBX1, SOX4, NR2F2, AKT1, QKI, SMAD7, SOX18, VEGFB*), and regulation of neuron projection development (*EFNB2, CDK5R1, RYK, RAPGEF1, CARM1, AKT1, PLZNA1, NCS1, DVL1, SLK, STK24, BRSK2, ADNP*). Interestingly, the canonical WNT signaling pathway was also an enriched biological pathway. WNT signaling plays an important role in endothelial cell proliferation, survival, differentiation and response to mechanical forces due to shear stress from blood flow.[23,24]

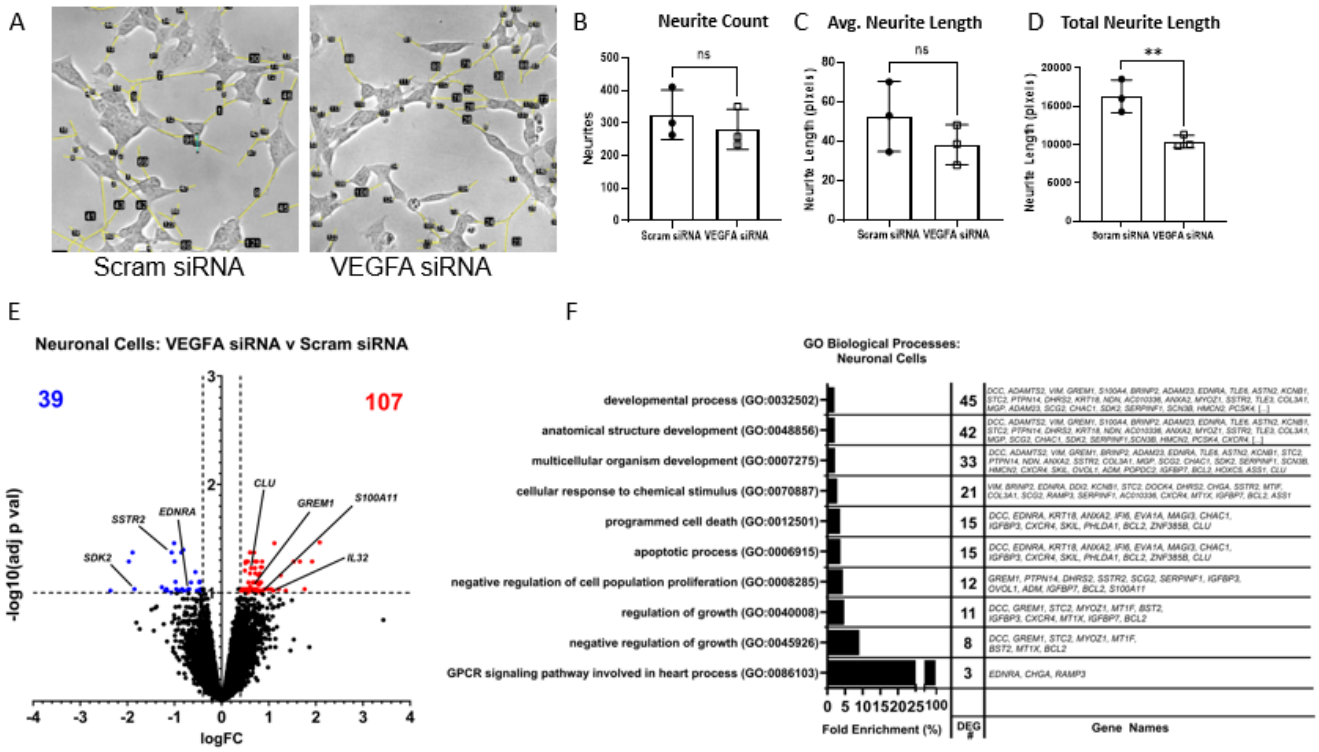

Fig. 6: VEGFA Inhibition Reduces *in vitro* Neurite Activity and Suppresses Processes Related to Growth and Elongation A) Neurite extension assay after treating neuronal cells with media collected from IL-1β stimulated and siRNA transfected human disc cells shows inhibition of neurites in neuronal cells (NC) with VEGFA siRNA treatment. B-D) Quantification of neurite lengths showing functional suppression with VEGFA siRNA in NCs. E) Volcano plot of RNA-seq analysis showing 146 differentially expressed genes and F) key biological processes regulated by VEGFA siRNA. NCs co-cultured with IL1β naïve disc cells showed undifferentiated cells possessing few short projections which cluster together, while NCs co-cultured with IL1β+SCRAM siRNA and NCs co-cultured with IL1β+VEGFA siRNA showed differentiated cells having many extensive projections.

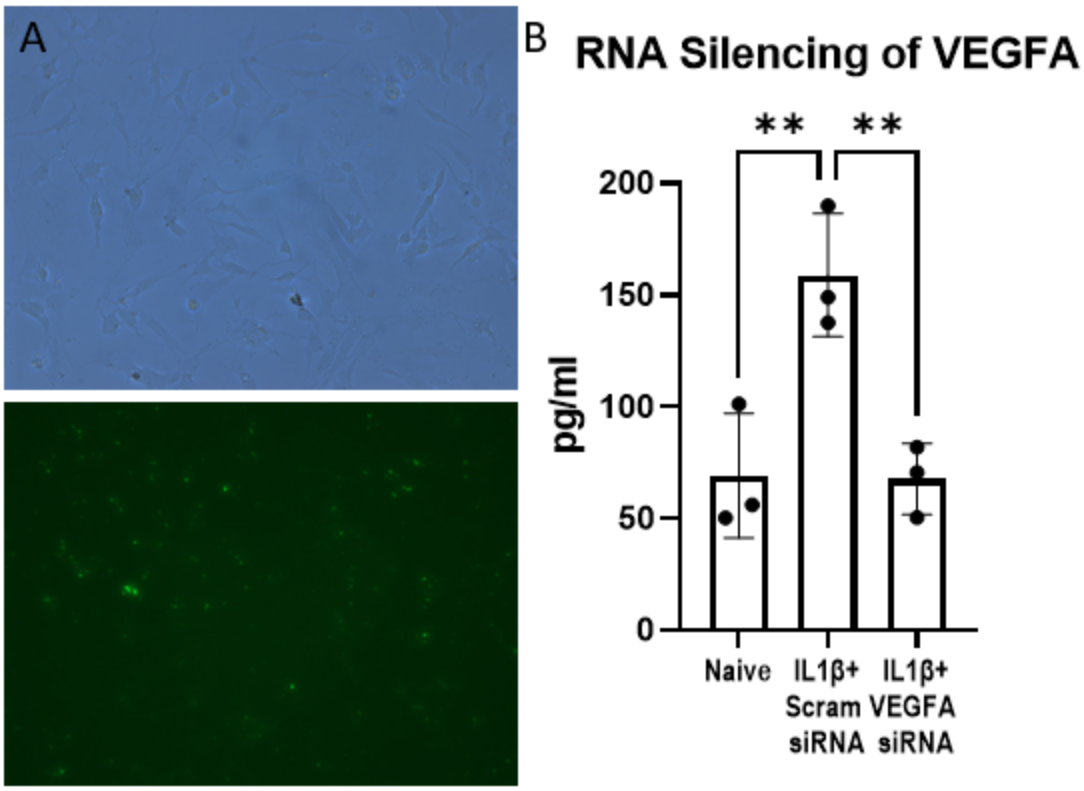

86

87 **Figure S6. Validation of VEGFA-siRNA Transfection in Disc Cells** A) Control siRNA (Fluorescein
88 Conjugate)-A revealed efficient transfection of cationic lipid-based transfection reagents in disc cells.
89 B) Stimulated disc cells by IL-1β with Scrambled siRNA show an increase in the VEGFA secretion
90 compared to naïve disc cells (p=0.04). Stimulated disc cells with IL-1β after being transfected with
91 VEGFA siRNA showed a significant silencing (57.4%) of VEGFA secretion compared to Scram siRNA
92 (p=0.03).

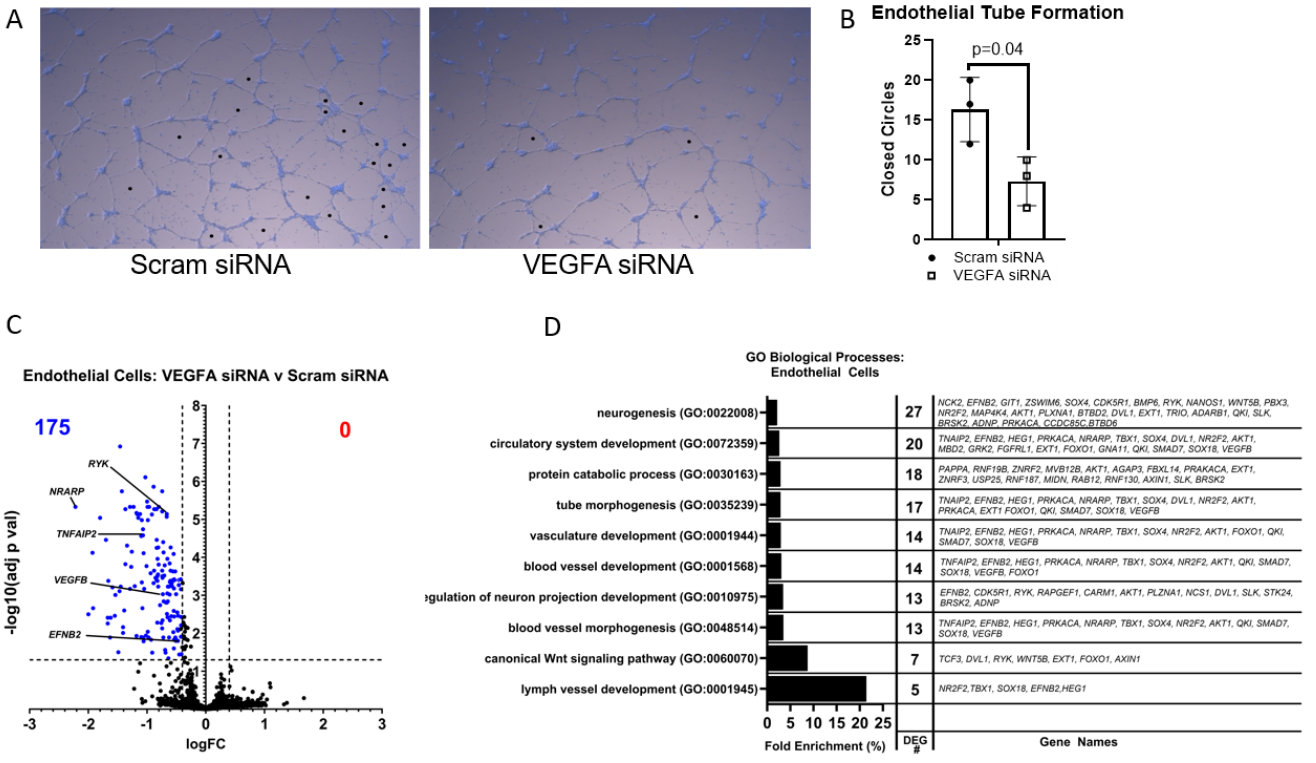

Fig. 7: VEGFA Inhibition Reduced *In Vitro* Endothelial Cell Function and Regulates Gene Transcription A) Matrigel tube forming assay images of endothelial cells (ECs) cocultured with human IVD cells treated with siRNA showing initiation of vessel formation after 6 hours. B) The silencing of VEGFA siRNA in IVD cells reduced tube formation in EC co-cultures, compared to IVD cells with Scrambled siRNA (p=0.04). C) The silencing of VEGFA in IVD cells via siRNA was associated with 176 downregulated genes in EC co-cultures. There is a suppression of key angiogenic genes in ECs including *HEG1*, *NARAP*, and *NCS1*. There is also a suppression of endothelial cell-derived neurogenic genes including *BRSK2* and *CRLF1*. D) The RNAseq analyses of the HMEC-1 also show an ontological shift to lymphangiogenesis, matrix remodeling, and suppression of neurovascular regulating pathways following co-culture with VEGFA-silenced IVD cells.

The endothelial cells co-cultured with the VEGFA-silenced IL-1β-stimulated IVD cells produce less angiogenic and inflammatory factors and more non-VEGFA proangiogenic compensatory factors

Following co-culture with VEGFA-silenced, IL-1β-stimulated IVD cells, the HMEC-1 endothelial cells exhibited a distinct cytokine profile that suggests a shift in cellular function. Notably, there was a reduction in secretion of VEGFA (Figure 8A) and CCL3 (Figure 8K) protein in the ECs co-cultured with VEGFA-silenced IVD cells, indicating decreased angiogenic and inflammatory signaling from factors secreted by the VEGFA-deficient IVD cells. In contrast, HMEC-1 cells exposed to VEGFA-silenced disc cells upregulated VEGFC protein, a canonical driver of lymphangiogenesis and lymphatic endothelial cell proliferation [25,26]. Simultaneously, ECs increased protein production of PDGF-AA (Figure 8J), a mitogenic factor that can compensate for VEGFA loss by promoting vessel stabilization and pericyte recruitment [27]. Increases in MMP1, MMP3, MMP10, and MMP13 protein levels (Figure 8C-F) reflect heightened extracellular matrix remodeling, a process essential for vessel pruning and structural reorganization typically associated with either vessel regression or tissue remodeling rather than active angiogenesis[28,29]. The elevation of granulocyte colony-stimulating factor (G-CSF) and granulocyte-macrophage colony-stimulating factor (GM-CSF) supports a role for immune cell recruitment and activation, especially of myeloid lineages that modulate inflammation and tissue repair (Figure 8G-H) [30,31]. Similarly, upregulation of CXCL1 and CCL5 (RANTES) reinforces the potential for leukocyte chemotaxis and immune surveillance (Figure 8I,L) [32,33].

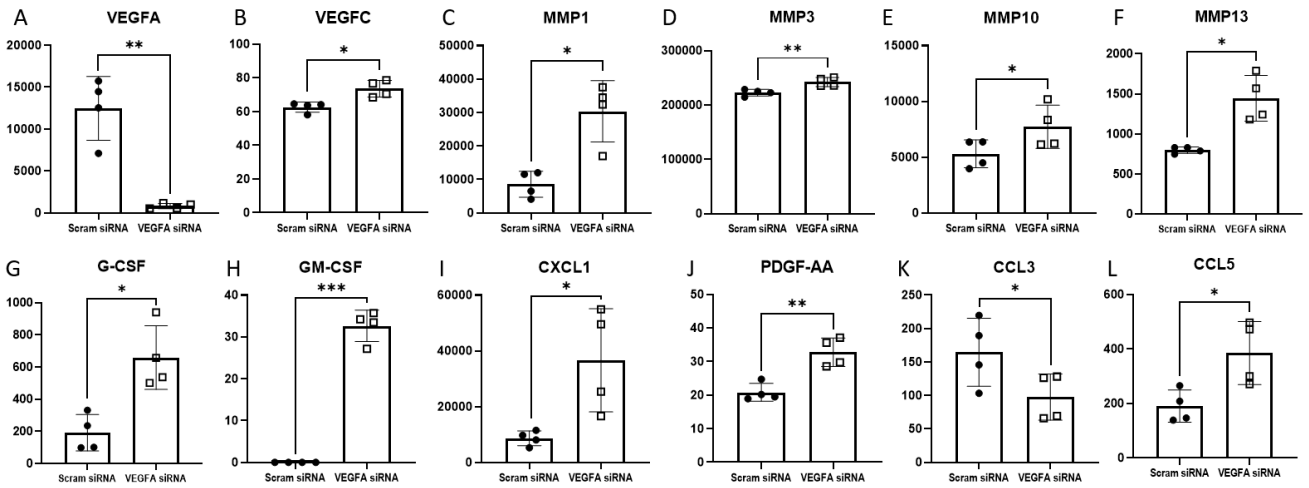

Fig. 8: The secreted factors from HMEC-1 (aka ECs) co-cultured with IVD cells were analyzed using the Luminex multiplex ELISA. Despite having a functional *VEGFA* gene, the ECs produced less (A) VEGFA and (K) CCL3 protein when co-cultured with *VEGFA*-silenced IL-1β–stimulated IVD cells. The ECs also produced more (B) VEGFC and (J) PDGF-AA that are both positive regulators of lymphoangiogenesis; MMPs (C-F; MMP1, MMP3, MMP10, MMP13) involved in matrix remodeling; chemokines including (G) G-CSF, (H) GM-CSF, (I) CXCL1, and (L) CCL5; and (J) PDGF-AA, a compensatory angiogenic growth factor. Units are pg/ml.

Group	Factor	Scrambled siRNA	VEGFA siRNA	p-value (paired)
Angiogenesis	Angiopoietin-2	29.1±2.1 (pg/ml)	28.9±2.4 (pg/ml)	0.53
Angiogenesis	Endoglin	84.8±10	92.9±5.9	0.06
Angiogenesis	Endothelin-1	337.3±42.5	336.7±34.9	0.84
Angiogenesis	Follistatin	436.8±485.1	915.9±1105.5	0.12
Angiogenesis	Leptin	70.4±11	70.4±8.4	0.79
Angiogenesis	PlGF	127.9±4	126.2±7.6	0.88
MMP	MMP2	8775±1081.8	9309.3±1816.7	0.55
MMP	MMP7	613.5±45.3	759.9±120.3	0.24
MMP	MMP8	138.6±116.4	239.4±120	0.30
MMP	MMP9	163±30.5	249.7±44.1	0.05
MMP	MMP12	582.4±65.1	604.9±59.9	0.60
MMP	TIMP1	100638.6±13530.7	89032.7±6718.9	0.13
MMP	TIMP2	30098.3±2192.1	31829.1±3278.2	0.07
MMP	TIMP3	3770.7±1298.2	2823.7±677.1	0.42
MMP	TIMP4	56.8±6.4	54.1±3.1	0.55
Cytokines	EGF	3.2±0.8	3.5±0.7	0.64
Cytokines	CCL11	7.7±0.6	7.6±0.7	0.89
Cytokines	FGF2	187±72.4	200.5±58.4	0.23
Cytokines	FLT3L	0.6±0.1	0.6±0.1	0.74
Cytokines	M-CSF	246.1±74.1	222.9±61	0.60
Cytokines	IL-6	2481.3±183	2518±201.4	0.94
Cytokines	IL-8	14958±894.4	16325.9±275.8	0.09
Cytokines	CCL2	3441.9±1491.7	3898.9±1275.8	0.18
Cytokines	PDGF-BB	32.9±7.5	20.9±5.8	0.45

Table S2**.** Panel of measured cytokines produced by the EC after co-culturing with the VEGFA-silenced IL-1β–stimulated human IVD cells.

Taken together, this cross talk supports a mechanism in which endothelial cells, in the presence of IL-1β-stimulated secretome of VEGFA-silenced IVD cells, pivot toward a reparative state characterized by elevated lymphangiogenesis, increased immune cell engagement, and enhanced matrix remodeling—rather than the robust angiogenic response seen with IL-1β-stimulated VEGFA-intact IVD cells. These findings align with the vessel-pruning and tissue remodeling hypotheses seen in regenerative contexts and suggest that VEGFA inhibition not only reduces angiogenesis but promotes a more immunomodulatory and matrix-adaptive endothelial phenotype. In addition, several mediators known to support vessel homeostasis (e.g., Angiopoietin-2, Endoglin, Endothelin-1, PlGF) remained

42 unchanged in co-culture with the VEGFA-silenced IVD cells (Table S2) and likely continue to support

43 the normal functions of existing vessels.

DISCUSSION

This is the first study to demonstrate that intradiscal innervation contributes to low back pain behavior and locomotive performance in a model of intervertebral disc degeneration. While studies in the past have shown progressive associations where neurovascular structures increase with progressive degeneration and pain,[34-38] none have been able to block or prevent these structures to prevent chronic pain and maintain locomotive performance. From this work, we also demonstrate that VEGFA may be a therapeutic target for a disease modifying therapy of low back pain. While VEGFA ablation did not significantly impact the structural and mechanical properties of the IVDs, it had a profound effect on neural and vascular infiltration and the subsequent mechanical sensitivity and locomotive performance following degeneration.

VEGFA plays a crucial role in limiting nerve and vessel infiltration post-injury. IVD degeneration in VEGFA-null mice exhibited reduced neurite and vessel lengths and the depths of their penetration, particularly in the outer annulus fibrosus (AF). VEGFA ablation inhibits the elongation and penetration of neural and vascular structures in the normally avascular IVD, potentially preventing painful sensory neurons from entering injured areas. The synergistic relationship between nerve and vessel infiltration highlights VEGFA's importance in neurovascular coupling within the IVD, with its absence leading to diminished neurite and vessel growth, which may limit painful neurological signals and affect overall disc health. These findings emphasize VEGFA's critical role in supporting neural and vascular initiation post-injury.

The loss of VEGFA also affected some of the neuropeptide-related signaling in in the Dorsal Root Ganglion (DRG). The increase expression of TrKA, TRPV1, and TRPA1 in the DRG have been observed in chronic low back pain [39,40], as well as in DRG that are sensitive to capsaicin stimulation [41]. The decrease in TrKA activation could be responsible for the reduction in pain sensitivity measured by

the Von Frey test. The VEGFA-null mice were less sensitive to mechanical filament provocation than the wild-type mice at prolonged time points. VEGFA removal also decreased TRPA1 expression, whose inhibition is associated with cold sensitivity, in the DRGs. However, these animals did not exhibit cold sensitivity. In contrast, TRPV1 expression, commonly associated with heat sensitivity [42], did not change between VEGFA-null mice and wild-type mice. Indeed, the VEGFA-null mice and wild-type mice did not exhibit observable difference in heat sensitivity in the hot plate experiment. The behavioral assessments revealed that despite exhibiting acute pain post-injury, VEGFA-null mice had improved recovery from mechanical sensitivity and avoided the prolonged sensitivity observed in WT mice. VEGFA-null mice did not develop the motor performance impairments seen in WT mice at later points (9-12 weeks), indicating a protective effect of VEGFA ablation against prolonged pain and impaired performance. Mechanical sensitivity showed imbalanced injury induced sensitivity while VEGFA inhibition balanced this asymmetry demonstrating that VEGFA loss rescued the IVD injury effects but did not change systemic pain sensing. Taken together, our results suggest that modulation of VEGFA in this context modifies the disease physiology rather than exerting analgesic effects.

Neurovascular Elongation vs Sprouting

Injuries to the intervertebral disc primarily trigger nerve and blood vessel sprouting as an adaptive response to inflammation and hypoxia [43,44]. This sprouting—stimulated by factors like NGF and inflammatory cytokines—leads to increased neurovascular infiltration into normally aneural and avascular disc regions, contributing to chronic pain and ongoing inflammation.[45-47] Consistent with this, we observed neurites and vessels infiltrating into the degenerating IVD at 3-weeks following injury. However, once sprouted, the neurites did not appear to elongate further, as evidenced by the relative similar lengths and depths between 3- and 12- weeks. In this animal model, VEGFA is ubiquitously ablated from the whole animal, and it is not possible to determine the source of the VEGFA. However,

our *in vitro* experiments support that blocking IVD-produced VEGFA is sufficient to prevent growth of the neurites and the maturation of the blood vessels. RNAseq analysis suggested that the reduced neural outgrowths is driven by the suppression of cell proliferation. We observed a phenotypic shift in the endothelial cells co-cultured with VEGFA-silenced IL-1β–stimulated IVD cells, which secreted higher levels of VEGFC and PDGF-AA, positive regulators of lymphangiogenesis, alongside increased MMPs, and immune cell recruiting chemokines. Such changes suggest that, in the absence of VEGFA-driven angiogenesis, endothelial cells promote a microenvironment conducive to tissue remodeling and immune-mediated repair. These immune cell recruiting chemokines are likely to be important for the intrinsic healing of the IVD [48]. RNAseq analyses of the HMEC-1 also showed an ontological shift to lymphangiogenesis and matrix remodeling with a suppression of key angiogenic genes including *Heg1, Narap*, and *Ncs1*. There is also a suppression of endothelial cell-derived neurogenic factors including *Brsk2* and *Crlf1*.

Needle stab injury models in animals are frequently utilized to study the pathophysiology of intervertebral disc (IVD) degeneration and to develop treatments for chronic lower back pain (CLBP). These models effectively replicate critical aspects of human disc degeneration, such as mechanical damage, inflammatory responses, and biochemical changes. For example, they simulate the mechanical damage caused by traumatic events and the inflammatory cytokine upregulation observed in human discs, which are crucial for understanding the progression of disc degeneration[49]. However, these models have limitations, especially in replicating the chronic, multifactorial nature of human CLBP and the complexity of human pain perception[50,51]. Human IVD degeneration occurs over years and decades, with the herniation of the IVD being one of the most apparent instigating factors. Despite the varied etiologies of discogenic pain, the chronic symptoms and eventual degenerative presentation, such as the deterioration of IVD structure, are quite similar. Therefore, the needle injury model in murine IVD is

13 employed to understand the mechanisms following IVD injury that eventually lead to low back pain
14 symptoms.

15 While these models are beneficial for basic research and initial therapeutic testing, their findings
16 must be interpreted with caution and validated in more complex models and ultimately in human clinical
17 studies. Differences in disc anatomy and biomechanics between humans and animals can affect the
18 translational relevance of these models, underscoring the need for complementary approaches to fully
19 capture the complexity of human IVD degeneration[51]. The needle injury in a mouse induces progressive,
20 but relatively rapid degeneration, occurring over weeks and months, compared to human degeneration,
21 which spans years and decades. Despite being traumatic relative to the human scale, this model is a
22 necessary caveat for developing feasible and mechanistic experiments. A single level lumbar injury
23 utilized here may also have underestimated the magnitude of our findings, since multiple groups have
24 shown a more pronounced pain behavior with 3 levels of injury in rodents [52].

25 The multifactorial nature of the injury and VEGFA ablation at 3 weeks complicated the detection
26 of significant changes acutely, but painful alterations were apparent with successive longitudinal
27 measurements. Additionally, the WT sham group displayed elevated disc degeneration scores,
28 suggesting that sham procedures may induce a mild phenotype. Notably, neurovascular ingrowth was
29 more pronounced on the dorsal side opposite the ventral injury location, as seen by others[34], likely due
30 to its proximity to the spinal cord and increased availability of neural and vascular sources. These
31 findings have translational promise since it is possible to intervene early in the sequalae of chronic low
32 back pain development. Since patients typically seek treatment only after an injury or an acute episode
33 of pain, the timely post-injury inhibition of VEGFA may be able to prevent the transition to chronic low
34 back pain.

35 Overall, the loss of VEGFA appears to be protective against mechanical sensitivity, with
36 decreased innervation and no major impact on IVD degeneration. These findings, for the first time to
37 date, show a causative relationship between neurovascular pathoanatomy and pain while implicating
38 VEGFA as a critical mediator in these processes following lumbar injury and highlight its potential as a
39 therapeutic target for preventing lower back pain through neurovascular inhibition.

40 **MATERIALS AND METHODS**

41 **Experimental Design**

42 *The Postnatal Inducible Ablation of Vegfa in Adult Mice*

43 Young adult, 4–6-month-old, ubiquitin (UBC)-Cre^{ERT2} ; *Vegfa*$^{fl/fl}$; Ai9-tdTomato mice on a C57BL/6J
44 background [53-55] allowed for a temporally controllable ablation of *Vegfa* upon tamoxifen administration
45 with recombination expressed via an Ai9 fluorescence reporter. An estrogen responsive Cre element is
46 activated when a mutant estrogen receptor (ERT2) renders Cre active upon tamoxifen binding and
47 promotes Cre entering the nucleus and catalyzing a recombination event at LoxP sites. These Cre+ mice
48 allow for precise temporal control over gene modification allowing ubiquitous recombination through
49 systemic ablation of *Vegfa* in all tissues. Moreover, this approach can avoid developmental defects and
50 embryonic lethality, especially in pathways that are essential to organogenesis. All procedures
51 (breeding, drug administration, procedures, and tissue extraction) were performed with WUSM IACUC
52 (Institutional Animal Care and Use Committee) approval.

53

54 *Confirmation and Quantification of Vegfa Ablation*

55 The Ai9-tdTomato reporter protein is co-expressed with Cre recombinase presence, and it is visually
56 evident (Figure S1) by inspection at the macroscopic scale after two doses of tamoxifen (100 mg/ kg)
57 administered over two consecutive days.

58 We also evaluated the efficiency of *Vegfa* ablation in the intervertebral disc (IVD) by measuring
59 the production of the VEGFA protein secreted by the IVD. Mice with Cre- and Cre+ alleles driven by
60 the ubiquitin promotor in animals with the homozygous *Vegfa* floxed alleles (UBC-Cre^{ERT2}; *Vegfa*$^{fl/fl}$
61 Ai9) received 2 consecutive days of tamoxifen administration via oral gavage (100 mg/kg in corn oil).

The animals were sacrificed on the third day, following the two days of induction. The functional spine units (FSUs), containing the vertebrae-intervertebral disc-vertebrae structure were cultured as previously described and stimulated with TNFα (5ng/ml) to provoke an inflammatory response [56]. Media was collected every other day for 7 days and analyzed using a VEGFA ELISA (R&D Systems Cat: DY493).

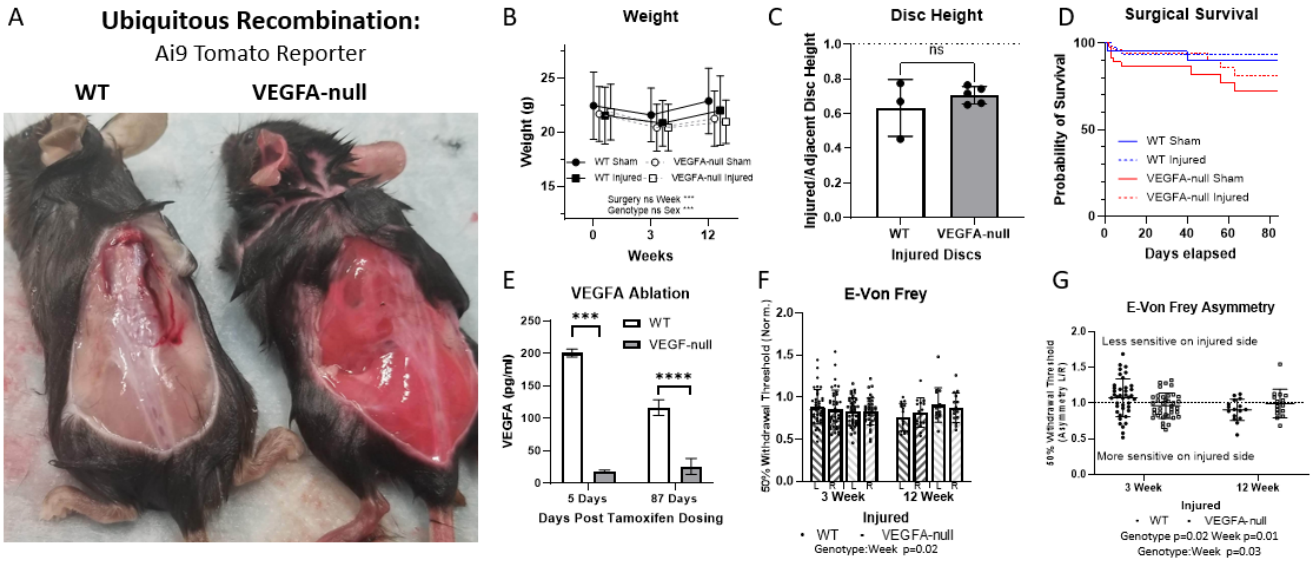

Figure S1 VEGFA ablation is highly efficient and does not pose notable health issues in the post-natal animal. A) Ubiquitous recombination in a WT and VEGFA-null showing the pink WT and red VEGFA-null Ai9 tdTomato reporter B) Mouse body weights at 0 (Baseline), 3 and 12 weeks remain similar between groups irrespective of genotype or surgery type C) Disc height ratio of injured/adjacent control disc height showing a similar decrease in heights following injury D) Surgical survival curves show no significant differences between genotype or surgery E) VEGFA ablation confirmation after initial ablation and 12 weeks from FSU media after TNFα stimulation ELISA showing a sustained ablation over time F) E-Von Frey shows that WT injured sensitivity increased over time (decreased withdrawal threshold) while VEGFA-null decreased over time (increased withdrawal threshold) G) E-

77 Von Frey asymmetry signifies an imbalance in WT mice that fluctuates over time while VEGFA-null
78 mice remained nearer to symmetry (dotted line). Data are presented as mean ± standard deviation.

79 *The Lumbar Puncture Intervertebral Disc Injury Model*

80 Male and female mice of 4-6 months of age were randomly allocated into respective experimental
81 groups. The animals undergoing surgery were first anesthetized using a subcutaneous lidocaine injection
82 (0.5% at 7mg/kg) followed by isoflurane inhalation (3–4% v/v induction and 2–2.5% v/v maintenance
83 at 1 L/min flow rate). The left flank was shaved, and the skin sterilized with 70% ethanol and povidone
84 iodine. Under microscopic guidance, a retroperitoneal dissection was performed to expose the lateral
85 aspect of the spine using a Penfield dissector and size 11 scalpels. The pelvis and hip were rotated
86 posteriorly to enhance the working space. The peritoneal wall was gently tugged to expose the psoas
87 muscle, which was retracted posteriorly to anteriorly using a cotton swab and then held in place with a
88 metal spatula. The spinal column and IVDs at the L5/6 and L6/S1 levels were exposed by blunt
89 dissection. The superior margin of the pelvic bone indicated the L6 vertebral body, confirming the
90 locations of L5/6 and L6/S1 IVDs. The L5/L6 IVD was targeted and either exposed in shams or injured
91 with a 30G needle 3 times through the annulus fibrosus and partially into the nucleus pulposus [20,34].

92 Postoperatively, mice were monitored every 8–12 hours for 4 days. Pain management included
93 intraperitoneal injections of carprofen (5 mg/kg) every 8–12 hours, supplemented with carprofen tablets
94 (2 mg/tablet) for 48-72 hours. On days 3 and 4 post-operatively, tamoxifen (TAM, Cat#: T5648,
95 Millipore Sigma) was given via oral gavage (100 mg/kg in corn oil, Cat#: C8267, Millipore Sigma)
96 to Cre+;*Vegfa*$^{fl/fl}$ animals (aka 'VEGFA-null') and Cre-;*Vegfa*$^{fl/fl}$ littermates ('WT') inducing *Vegfa*
97 ablation. Data collection occurred at 3 and 12 weeks with behavioral assays including additional
98 timepoints at baseline, within 7 days of injury, and longitudinal cohorts at 6 and 9 weeks. Mouse weights

99 were collected at baseline, 3, and 12 weeks to track overall health and survival was tracked throughout
00 the experiment to create Kaplan-Meier survival curves.

01 Acute 3-week post-op and chronic 12-week post-op time points were chosen with the acute
02 injury response allowing for the initial surgical wound healing recovery, while chronic LBP is defined
03 as pain lasting 12 weeks or longer [57,58].

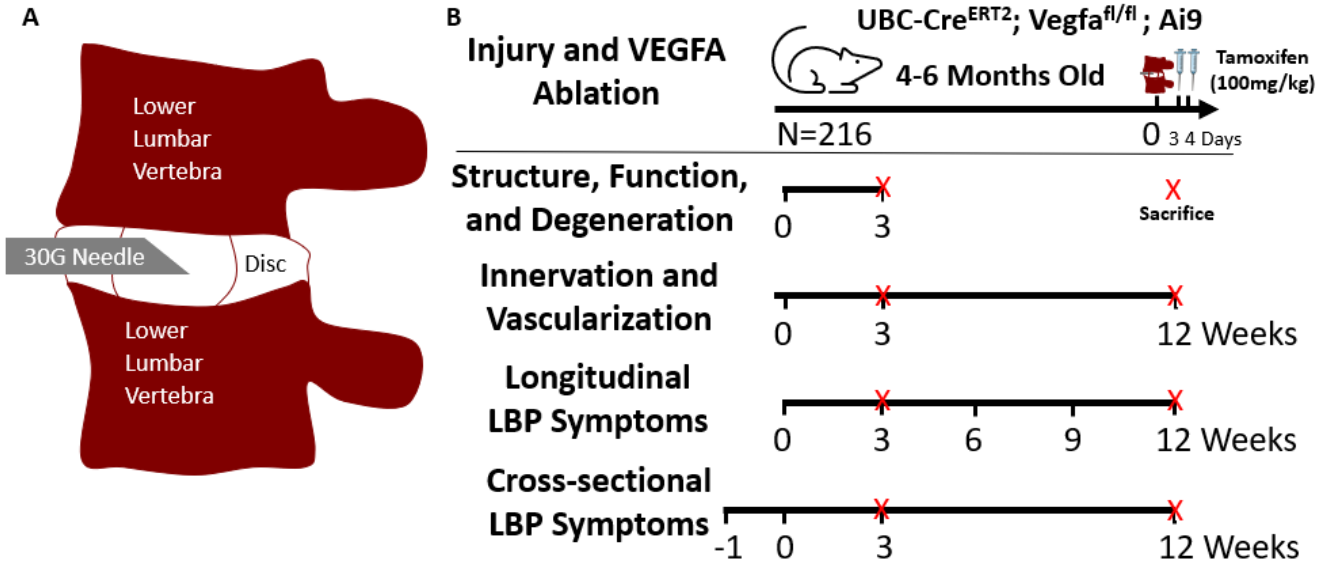

04

05 **Figure S2: Experimental Design** A) Lower lumbar disc puncture model showing the relative scale of
06 a 30G needle and the depth of injury B) Experimental design for various outcomes including injury at
07 time=0 with VEGFA ablation at 3-4 days post-op, and acute and chronic terminal time points at 3 and
08 12 weeks. Baseline behavior within one week or surgery normalized behavioral outcomes. N=216 total
09 mice.

10 **Histological analyses**

11 *Histopathological Evaluation of Degeneration*

12 To quantify acute IVD degeneration at 3 weeks, frozen 10 µm thick midsagittal sections were stained
13 with Safranin O / Fast Green and imaged at 10x on a Nanozoomer (Hamamatsu, Japan).
14 Histopathological scoring followed an established protocol for degeneration in four compartments of

the IVD including the NP, AF, end plate, and interface/boundary regions [59]. Mean degeneration scores from three independent investigators (n=3/sex/genotype/surgery, N=24 total) were used for analysis.

Structural Quantification of Nerve and Vascular Features by Immunohistochemistry

Spines from the animals were fixed in 4% paraformaldehyde for approximately 48 hours, washed 6 times for 15 minutes each in 1X PBS, and subsequently demineralized in 14% EDTA for 10-14 days. After which, samples were washed 8-10 times for 15 minutes in 1X PBS and serially infiltrated with 10%, 20%, and 30% sucrose solutions for 1 hour each prior to optimal cutting temperature (OCT) infiltration and freezing for cryosectioning. Section thickness was 50 µm to provide a semi-3-dimensional visualization of the neuronal and vascular morphology. Serial sections were collected with CryoJane adhesive slides to adhere tissue to the slide during IHC staining with tissues being stored at -80°C prior to antibody staining.

To stain for Protein Gene Product 9.5 (PGP9.5), Endomucin, and DAPI counter stain, a 4-day protocol[60] was followed whereby slides were dried at room temperature for 30 minutes and washed in PBS 2 times for 5 minutes. A PAP pen was used to create a hydrophobic perimeter around the tissue and allow for direct pipetting of reagents onto the slides to avoid tissue loss from vertical slide immersion. Slides were blocked with 10% donkey serum and 0.3% Triton X-100 in PBS for 1 hour at room temperature. The primary PGP9.5 antibody (Millipore Cat # Ab1761) at a 1:1000 dilution and Endomucin antibody (Cat #14-5851-85) at a 1:500 dilution was added to 1% normal donkey serum in a TNT (Tris-NaCl-Tween) buffer and incubated 48 hours at 4°C in a humidified chamber. Samples were then washed 3 times for 5 minutes in TNT buffer prior to incubation of a PGP9.5 secondary antibody (Jackson Cat #711-545-152) at 1:1000 concentration and 488nm fluorophore and Endomucin secondary antibody (Jackson Cat #712-605-153) at 1:1000 concentration and 657nm fluorophore in 1% normal donkey serum in TNT buffer

for 24 hours at 4°C in a humidified chamber. Samples were washed 3 times with TNT for 5 minutes prior to DAPI (Sigma-Aldrich D9542) at 1:1000 for 5 minutes at room temperature. A final wash with TNT 3 times for 5 minutes was done prior to cover slipping and subsequent sealing of the slides with Fluoromount-G a day later (Thermo Cat:00-4958-02).

To confirm that the PGP9.5 positive structures within the IVD accurately captured the sensory neurons population, we conducted a direct comparison of the PGP9.5 straining of an injured intervertebral disc in a $Na_v1.8$ td Tomato reporter mouse and found the $Na_v1.8$+ features accounted for 88% of the PGP9.5+ features with a spatial colocalization correlation of R=0.86 (Figure S3). The sodium-sensitive ion channel $Na_v1.8$ is highly specific to sensory neurons [61-63].

DAPI, PGP9.5, and Endomucin helped visualize, respectively, cell nuclei, broad neural populations, and endothelial cells of vasculature via a confocal microscope (Leica, USA) at 2.5 µm focal depth increments with 10x magnification and 2048x2048 resolution and 600 speed with 2 frame averaging. Excitation and emission wavelengths were set as follows: DAPI excitation 405nm and emission 414-450 nm, PGP9.5 excitation 488nm and emission 498-530 nm, and Endomucin excitation 635nm and emission 650-725 nm. Note that there was no overlap between the Ai9 tdTomato reported with excitation of 554 and emission of 581nm. Neurite and vessel quantification of the outer AF were performed on max projections of a Z-stack with Fiji (ImageJ), with lengths on or within the AF and the surrounding fibrous tissue calculated from the Neuroanatomy SNT plugin and with depths calculated normal to the peripheral edge of the AF. PGP9.5 staining showed some non-specific regions so was only not included if neuronal morphology was apparent.

To quantify spatial coupling of neurites and vessels, an automated MATLAB program was developed to measure lengths and depths and calculate colocalization lengths and a colocalization ratio based on distance from the rare neurite features. Spatial coupling was defined as vessels within 30 µm from neurites and based on the distance between two adjacent lamellae as lamellar structure and proximity likely impact the transmission of neurovascular coupling signaling.

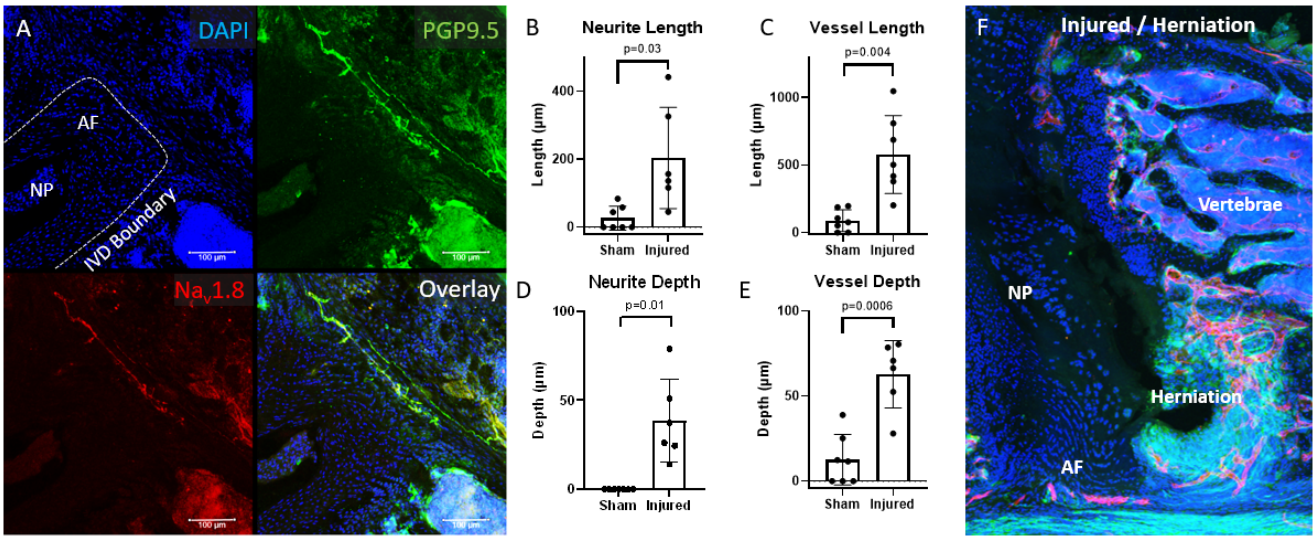

Figure S3: Validation of Neuronal Stain with Injury A) Validation of PGP9.5 IHC with a Na_v 1.8-TdTomato reporter showing the coincidence of the more specific sensory Na_v 1.8 with pan neuronal PGP9.5. Na_v1.8+ features accounted for 88% of the PGP9.5+ features with a spatial colocalization correlation of R=0.86. B-E) Acute (3 week) neurite length and depth and vessel length and depth data showing the increased lengths associated with injured discs F) IHC of a herniated disc at 3 weeks showing diffuse non-specific green PGP9.5 staining and red Endomucin vessels. Data are presented as mean ± standard deviation.

Neuropeptide Immunostaining of the Dorsal Root Ganglia

Frozen DRG sections, isolated from L1-L3 were processed for immunohistochemistry using a standardized protocol across all targets. Briefly, slides were fixed in 4% paraformaldehyde for 10

77 minutes at room temperature. After washing in 0.1 M Tris buffer (pH 7.6), non-specific binding was
78 minimized through sequential blocking steps with 0.005% BSA in Tris and 10% normal goat serum.
79 Sections were incubated overnight at 4°C with primary antibodies—anti-TrkA (1:100, Alomone Labs
80 #ANT-018), anti-TRPA1 (1:200, Alomone Labs #ACC-037), or anti-TRPV1 (1:500, Abcam
81 #ab6166)—diluted in Tris-BSA. After rinsing, a goat anti-rabbit Alexa Fluor 488 secondary antibody
82 (1:300, Invitrogen #A11006) was applied for 4 hours at room temperature or overnight at 4°C. Nuclear
83 counterstaining was performed using DAPI (1:5 dilution in 0.1 M Tris), and slides were mounted prior
84 to imaging. DRG immunohistochemical images were quantified using the custom Python software,
85 DRGVisual. Contrast Limited Adaptive Histogram Equalization (CLAHE) was applied to enhance the
86 contrast of the images. The processing began with Canny edge detection to refine the segmentation and
87 ensure accurate depiction of cell boundaries. Following edge detection, seed points within the cells were
88 identified to indicate the center of the cells, and diameters were drawn to estimate each cell's maximum
89 size. Cell regions were grown using a projection-based region-growing algorithm that expands the
90 region from each seed point by examining neighboring pixels and including them in the region if they
91 meet criteria based on intensity and connectivity. For each cell, the corrected total cell fluorescence
92 (CTCF) was calculated by subtracting the background intensity from each pixel's intensity within the
93 cell region and summing the total fluorescence across the cells for each ion channel.

94 **3D Structural Evaluation of Intervertebral Disc Structure Using Contrast-enhanced µCT**

95 At 3 weeks post lumbar intervertebral disc injury, in vivo µCT was used to evaluate structural changes
96 of the intradiscal space (VivaCT, 45 kVp, 177 uA, 300 ms integration time, 10 µm voxel) with isoflurane
97 inhalation (2-3% v/v). Disc height was calculated in ImageJ as the average of 5 measures across the
98 midsagittal view [20]. To confirm that the loss of VEGFA did not affect the structure of the IVD, we
99 examined the uninjured L4-L5 and L6-S1 IVDs between the VEGFA-null and the WT animals.

Additionally, we examined the injured L5-L6 IVD level to ensure that the VEGFA-null animals were susceptible to injury-mediated degeneration. A 2-tailed t-test was used to determine differences between groups.

The structural changes at this 3-week post injury time point were further evaluated using the e*x vivo* contrast-enhanced micro-computed tomography (CEμCT). Ioversol was used as a contrast agent to highlight the water-rich nucleus pulposus [64]. The fresh IVDs were immersed in 50% Ioversol (OptiRay 350, Guerbet Pharma) at 37°C for 24 hours before imaging. The Scanco40 μCT system (Zurich, Switzerland) scanned samples at 45 keVp, 177 μA, 10.5 μm voxel size, and 300 ms integration after the incubation [65]. Groups were n=3 mice/sex/genotype/injury. Total disc ROI and nucleus pulposus ROI were contoured using the MATLAB graphical user interface from Washington University Musculoskeletal Image Analyses (github.com). NP hydration, a ratio of nucleus attenuation to total disc attenuation (NI/DI), was calculated along with volumes and disc height index, DHI, as an average of 5 height measures in a midsagittal slice over the disc width.

Biomechanical Assessment of the Intervertebral Disc

Mechanical behavior of the IVDs using dynamic compression testing under displacement control was conducted using a BioDent reference point indenter (Active Life Scientific) [66]. After CEuCT, these samples (n=3 mice/sex/genotype/injury) were mechanically tested with the strain rate calculated from the 5-point average disc height. FSUs were affixed to aluminum platens and immersed in a phosphate-buffered saline bath at room temperature and preloaded to 0.25N. A sinusoidal compressive waveform at 10% strain and 1 Hz frequency was applied for 20 cycles. The average stiffness was calculated from the second through the final loading cycles and the loss tangent, or dissipation factor, was calculated from the phase angle between load and displacement data.

Behavioral Assessments

Habituation measures were taken to reduce animal stress during behavioral assessments. Acclimation to room environment prior to assessment was set for 1 hour at the beginning of each behavioral testing week. To avoid additional animal stress, assessments were typically performed twice a day with 1 hour rest between tests between 9am-5pm to minimize diurnal variations in activity [67]. All tests were performed by the same laboratory personnel. Baseline data was collected one week prior to surgery and post-operative data collection included a cross-sectional group at baseline, 3, and 12 weeks and a longitudinal group at 3, 6, 9, and 12 weeks. Care was taken to ensure a clean, quiet, and odor-free environment at a controlled temperature (20-23°C). Testing was initiated up to one week prior to the 3- and 12-week time points as the full set of assays took 4-5 days to complete with efforts made to reproduce the order and timing of each test to remove stress on the animals and replicate methods.

Mechanical Sensitivity Measured Using the Von Frey and E-Von Frey

Mechanical sensitivity was measured using the up-down method of the Von Frey test using Semmes Weinstein filaments (Bioseb, France) and an electronic Von Frey (BIOSEB, France) [68,69]. Prior to baseline behavioral testing, mice were habituated to the elevated mesh grid chamber for 1 hr. Calibrated filaments were applied to the plantar surface of the hind paw to elicit paw withdrawal or filament buckling [70]. Filament Von Frey was done on the left hind paw to focus on the injury response. EVF consisted of maximum force values at withdrawal from the median of the result of 3 trials which were conducted bilaterally, with at least 5 min between testing opposite paws, and at least 10 min between testing the same paw. Post-op measures were normalized to baseline.

Hot and Cold Nociceptive Sensitivity

Mice were subjected to thermal stimulus to measure the temperature sensitivity response [71,72]. A hot/cold plate (Bioseb, France) was set to 55±0.5°C or 5±0.5°C and mice were placed individually onto the plate with a transparent enclosure to prevent escape and allow for visibility. The latency to the first sign of nociceptive behavior, either lick of the hind paws or jumping for hot plate and lifting, licking, or shaking of the hind paws for cold plate was recorded with a cutoff time of 20 seconds for hot or 30 seconds for cold to prevent tissue damage. Three repeated measures were collected with >15 minutes between tests to allow for home cage recovery. Values were averaged and normalized to baseline.

Functional Assessments of Performance

Locomotor Function – Rotarod

Assessing motor coordination and balance, the Rotarod performance test challenged mice to a rotating rod apparatus (Bioseb, France) [69,73,74]. Prior to testing, mice were trained on the Rotarod at a slow 4 rpm for 2 minutes to ensure baseline capabilities. Mice unable to achieve this baseline capacity were excluded from assessment. On a subsequent day, mice were tested on an accelerating bar from 4 to 40 rpm over a 2-minute period. Latency to fall was recorded for each mouse. Each mouse underwent 5 trials with a >5-minute rest period between trials to reduce fatigue. The best performance of the 5 trials was used for data analysis and normalized to baseline when possible.

Open Field Testing

In the open field test, designed to evaluate exploratory passive behavior, mice were individually introduced into the center of an open field arena (40 cm x 40 cm, with 30 cm high walls) equipped with an automated tracking system (Omnitech Electronics, Columbus, OH) [69,73,74]. The apparatus featured an array of infrared sensors for precise movement tracking over a 60-minute test period. Behavioral

67 parameters recorded included total distance traveled and instances of vertical rearing, among others. The
68 total distance and rearing events were reported over 60 minutes.

69 Strength

70 *Inverted Wire Hang Endurance*

71 In the wire hang behavioral test, mice were evaluated for neuromuscular strength and endurance [75]. The
72 apparatus consisted of a wire mesh (2 mm diameter) suspended above a soft bedding layer to ensure a
73 safe landing for the mice. Each mouse was gently held by the base of the tail and allowed to grasp the
74 wire at a 60° incline before the mesh was inverted to 180°. The duration the mouse remained suspended
75 inverted was recorded up to a maximum of 2 minutes. A minimum 5-minute rest was given between
76 trials. The maximum time of three trials was recorded.

77

78 *Grip Strength*

79 Grip strength, a measure of neuromuscular strength, was measured using a uniaxial grip force tester
80 (Bioseb, France) [76]. Hind paw grip strength assessed mechanical strength as the mouse was gently
81 restrained and allowed to freely grab and hold a bar with both hind paws. Maximum force was recorded
82 as the tail was pulled in a steady manner to avoid rate-dependent effects. A brief rest period, >15 sec,
83 was given between each of the 5 repeated trials. Average strength was reported normalized to body
84 weight at the time of testing and normalized to baseline.

85

86 **Cell Culture**

87 *Human Primary IVD Cell Culture*

88 Human intervertebral disc cells were isolated from the disc tissue of eight patients (mean age ± SD =
89 68.5 ± 8.1; female:male = 5:3; mean Pfirrmann grade ± SD = 3.5 ± 0.7) removed during elective

90 discectomy surgeries (Table S3). Human biospecimens were obtained under IRB Exemption Category
91 4, in accordance with institutional and federal guidelines for research using de-identified, previously
92 collected samples, as described in prior studies [77,78] . Tissue specimens were placed in sterile Ham's F-
93 12 medium (F-12; Gibco-BRL, Grand Island, NY) containing 1% penicillin/streptomycin (P/S; Gibco-
94 BRL) and 5% fetal bovine serum (FBS; Gibco-BRL). Disc tissue was washed three times with Hank's
95 balance salt solution (HBSS; Gibco-BRL) containing 1% P/S to remove blood and other bodily
96 contaminants prior to isolation. Specimens were minced and digested for 60 min at 37°C under gentle
97 agitation in F-12 medium containing 1% P/S, 5% FBS, and 0.2% pronase (Calbiochem, La Jolla, CA).
98 The specimens were rinsed three times with HBSS and 1% P/S and incubated overnight in a solution of
99 F-12 medium containing 1% P/S, 5% FBS, and 0.025% collagenase I (Sigma Chemical Co, St. Louis,
00 MO). A sterile nylon mesh filter (70 µm pore size) was used to separate suspended cells from the
01 remaining tissue debris. Isolated cells were centrifuged (2000 rpm, 5 min) and resuspended in F-12
02 medium with 10% FBS and 1% P/S. Cells were plated in a 75-cm^2 culture flask (VWR Scientific
03 Products, Bridgeport, NJ) and incubated at 37°C, 5% CO^2, 20% O^2 in a humidified incubator. Culture
04 medium was changed three times weekly, and cultures grew to 90% confluence. Cells were then
05 trypsinized (0.05% trypsin/ethylene diaminetetraacetic acid; Gibco-BRL) and re-plated (6 x 10^5
06 cells/mL) in 75-cm^2 culture flasks.

		Pfirrmann Grade								Endothelial Cell (RNA/ multiplex/ ELISA)	Matrigel Outgrowth Assays	with Neural Cell (RNA/neurite)
Age	**Sex**	**T12/L1**	**L1/2**	**L2/3**	**L3/4**	**L4/5**	**L5/S1**	**Mean**	**STD**			
70	F		3	3	4	4	4	3.6	0.5		X	
73	F			3	3	4	5	3.8	1.0	X		
73	M			3	3	3	4	3.3	0.5			X
66	F	3	3	3	5	5		3.8	1.1	X	X	
50	M					3	4	3.5	0.7	X		
76	F		2	3	3	4		3.0	0.8			X
68	F					3	3	3.0	0.0			X
72	M	3	3	4	4	4	5	3.8	0.8		X	

Table S3: Patients' Demographics for Disc Cells (DCs): DCs were isolated from the disc tissue of eight patients removed during elective surgical procedures for degenerative spinal disease. Pfirrmann Grades for T12/S1 are shown along with assay distributions for each patient sample.

Immortalized Human Microvascular Endothelial Cell (HMEC-1) Culture

HMEC-1(CRL-3243; ATCC, Masassas, VA) were cultured in MCDB 131 medium (10372019; Gibco-BRL) containing 10 ng/mL epidermal growth factor (PHG0311; Thermo Fisher Scientific, Waltham, MA), 500 mg/mL hydrocortisone (H0396; Sigma), 1% P/S, 2 mM L-Glutamine and supplemented with 10% FBS. Cells at passage number 5-10 were plated in 75 cm^2 culture flasks and grown to 90% confluence.

Immortalized Human Neuroblastoma Cell (SH-SY5Y) Culture

The SH-SY5Y human neuroblastoma cell line (CRL-2266; ATCC) was cultured in a 1:1 mixture of Eagle's Minimum Essential Medium (EMEM; ATCC, Manassas, VA) and Ham's F12 medium, supplemented with 10% FBS and 1% P/S in a 5% carbon dioxide humidified incubator at 37°C. Cells at passage number 5-10 were plated in 75 cm^2 culture flasks and grown to 90% confluence.

21 *Vascular Endothelial Growth Factor (VEGF)-siRNA Transfection*

22 Isolated human IVD cells were seeded in 6-well plates at a density of $3x10^5$ cells per well 24 hours prior
23 to transfection. VEGF-specific siRNA (sc-29620; Santa Cruz Biotechnology, Dallas, Tx) and scrambled
24 control siRNA- FITC (sc-36869; Santa Cruz Biotechnology) were transfected into DCs using
25 Lipofectamine™ RNAiMAX Transfection Reagent (Catalog #: 13778100, Thermo Fisher) following
26 the manufacturer's protocol. The final concentration of siRNA in the culture medium was 50 pM. The
27 effectiveness of transfection was evaluated by checking the amount of the secreted VEGF in media using
28 ELISA (DY293; R&D system, Minneapolis, MN) and confirming transfection of control siRNA by
29 FITC fluorescence with a Nikon Eclipse Ti2 inverted scope at 10x.

30 *Co-culture between IVD cells and HMEC-1 (ECs) Cells*

31 IVD cells were plated in a 6 well plate and transfected with either control, scrambled siRNA (Scram
32 siRNA) or with VEGF specific siRNA (VEGF siRNA). Medium with 1% FBS and recombinant human
33 interleukin-1β (IL-1β; R&D Systems) at 1 ng/mL was added to stimulate Scram siRNA (IL-1β+Scram
34 siRNA) and VEGF siRNA (IL-1β+VEGF siRNA) transfected IVD cells for 24 hours. After stimulation,
35 HMEC-1 cells "ECs" that were plated for 24 hours on 1 μm pore co-culture inserts (Thincert cell culture
36 insert; Greiner, Monroe, NC) at a density of $3x10^5$ cells were inserted to the wells containing Scram
37 siRNA or VEGF siRNA transfected IVD cells with MCDB media plus 1% FBS. ECs co-cultured with
38 stimulated Scram siRNA treated IVD cells are denoted as $EC_{IL\text{-}1\beta+Scram\ siRNA}$ and ECs co-cultured with
39 stimulated VEGF siRNA treated IVD cells are denoted as $EC_{IL\text{-}1\beta+VEGF\ siRNA.}$ Naïve ECs that did not
40 undergo co-culturing were used as a control group. ECs were analyzed via a Matrigel tube formation
41 assay, multiplex (Human Angiogenesis & Growth Factor 17-Plex, Human Cytokine Panel A 48-Plex,
42 Human MMPTIMP 13-Plex. MilliporeSigma) and RNA sequencing (Figure S4).

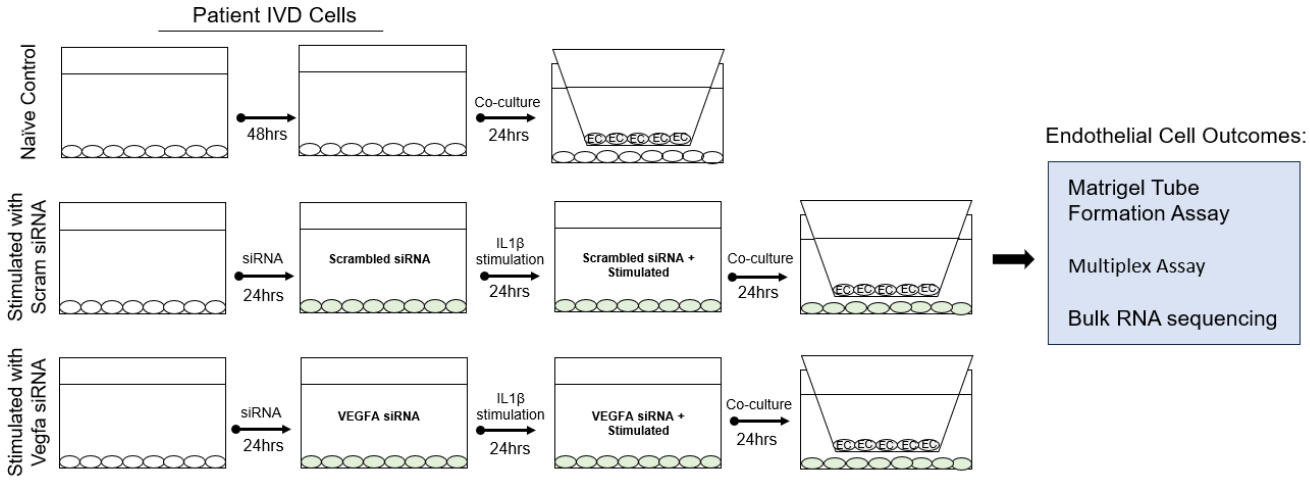

Figure S4. Schematic drawing of Co-culture between Disc Cells (DCs) and HMEC-1(ECs) DCs were plated on a 6 well plate left as naïve or transfected with Scrambled control siRNA (Scram siRNA) or VEGFA specific siRNA (VEGFA siRNA) for 24 hours. Cells were then treated with 1 ng/mL of IL-1β to stimulate the Scram siRNA and VEGF siRNA transfected DCs (IL-1β+Scram siRNA or siRNA IL-1β+VEGF siRNA, respectively) for 24 hours but the naïve DCs were left unstimulated. After stimulation, 1 µm pore co-culture inserts plated with ECs were inserted into each well for direct coculturing for 24 hours.

Co-culture Between IVD cells and SH-SY5Y Cells (NCs)

SH-SY5Y neuronal cells "NCs" were plated at a density of 1.5 x 10^5 cells per well in a 6 well plate and cultured for 48 hours prior to the co-culture experiment. For co-culturing, non-stimulated IVD cells "naive", IL-1β+Scram siRNA, and IL-1β+VEGF siRNA transfected IVD cells were plated on the co-culture insert at a density of 3.0 x 10^5 cells and co-cultured for 48 hours with NCs. NCs were analyzed via a neurite outgrowth assay and RNA sequencing. (Figure S5)

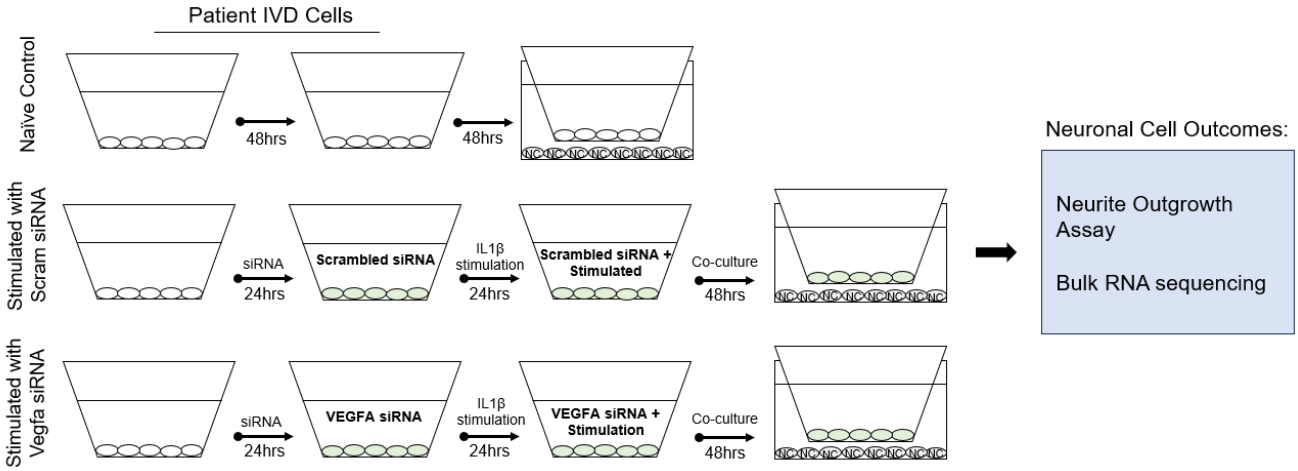

Figure S5. Schematic drawing of Co-culture between Disc Cells (DCs) and SH SY5Y cells (NCs). NCs were plated on a 6 well plate and cocultured with 1 µm pore co-culture inserts plated with DCs 48 hours. DCs were either left as naïve or transfected with Scrambled control siRNA (Scram siRNA) or VEGFA specific siRNA (VEGFA siRNA) for 24 hours. The naïve DCs were left unstimulated and the Scram siRNA and VEGF siRNA transfected DCs were stimulated with 1 ng/mL of IL-1β (IL-1β+Scram siRNA or siRNA IL-1β+VEGF siRNA, respectively) for 24 hours before coculturing.

RNA Preparation and Sequencing

Post co-culture experiments, HMEC-1 and SH-SY5Y cells were lysed (TRIzol reagent, Fisher Scientific), and total RNA was extracted (Direct-zol RNA MicroPrep Kit, Zymo Research). Samples were prepared according to library kit manufacturer's protocol, indexed, pooled, and sequenced on an Illumina NovaSeq X Plus. Basecalls and demultiplexing were performed with Illumina's DRAGEN and BCLconvert version 4.2.4 software. RNA-seq reads were then aligned to the Ensembl release 101 primary assembly with STAR version 2.7.9a1. Gene counts were derived from the number of uniquely aligned unambiguous reads by Subread:featureCount version 2.0.32. Isoform expression of known Ensembl transcripts were quantified with Salmon version 1.5.23. Sequencing performance was assessed for the total number of aligned reads, total number of uniquely aligned reads, and features detected. The

76 ribosomal fraction, known junction saturation, and read distribution over known gene models were
77 quantified with RSeQC version 4.04. All gene counts were then imported into the R/Bioconductor
78 package EdgeR5 and TMM normalization size factors were calculated to adjust for samples for
79 differences in library size. Ribosomal genes and genes not expressed in the smallest group size (minus
80 one sample greater than one count-per-million) were excluded from further analysis. The TMM size
81 factors and the matrix of counts were then imported into the R/Bioconductor package Limma6.
82 Weighted likelihoods based on the observed mean-variance relationship of every gene and sample were
83 then calculated for all samples and the count matrix was transformed to moderated log 2 counts-per-
84 million with Limma's voomWithQualityWeights7. The performance of all genes was assessed with
85 plots of the residual standard deviation of every gene to their average log-count with a robustly fitted
86 trend line of the residuals. Differential expression analysis was then performed to analyze differences
87 between conditions and the results were filtered for only those genes with Benjamini-Hochberg false-
88 discovery rate adjusted p-values less than or equal to 0.05. The raw data files are available on the Gene
89 Expression Omnibus database: GSE294577
90
91 See Excel files
92 Table S8A,B and S9A,B: DEGs and GO terms for Endothelial and Neuronal Cells
93

94 *Multiplex Protein Assay*

95 The supernatant from naive ECs and those co-cultured with IL-1β+Scram siRNA and IL-1β+VEGF
96 siRNA transfected IVD cells was collected and analyzed by multiplex protein assay (Human
97 Angiogenesis & Growth Factor 17-Plex, Human Cytokine Panel A 48-Plex, Human MMPTIMP 13-

98 Plex, Eve Technologies, Calgary, Alberta, Canada). Out of range values or results < 2pg/ml were not
99 included.
00
01 *Matrigel Tube Formation Assay*
02 To determine the vessel formation capacity between ECs cultured with conditioned media (CM)
03 collected from IL-1β+Scram siRNA versus IL-1β+VEGF siRNA transfected IVD cells, a Matrigel tube
04 formation assay was performed. Matrigel matrix (356231; Corning Inc., Corning, NY), a gelatinous
05 protein mixture that mimics the extracellular matrix, was used to coat a 24-well plate following the
06 manufacturer's protocol. HMEC-1 cells at the density of 3 x 10^4 cells per well were suspended in the
07 CM collected from IL-1β+Scram siRNA or IL-1β+VEGF siRNA transfected IVD cells for 48 hours and
08 plated onto each Matrigel coated well. Images were acquired at 6 hours and 12 hours post plating via a
09 Nikon Eclipse Ti2 inverted scope at 10x. To assess the ability of tube formation by each conditioned
10 media and time point, the numbers of closed loops were counted.[79]
11
12 *Neurite Outgrowth Assay*
13 The number and length of neurites from NCs co-cultured with non-stimulated IVD cells "naive", IL-
14 1β+Scram siRNA, or IL-1β+VEGF siRNA transfected IVD cells were compared. Neurite outgrowth
15 was quantified using ImageJ software. For each neuron, neurite number and length were counted
16 manually. Neurite length was measured from the edge of the cell body to the tip of the neurite. The
17 average neurite length per neurite was calculated for each treatment group, with all measurements
18 expressed in microns.

19 **Statistical and Bioinformatics Analyses**

20 Statistical comparisons on repeated measures, IE longitudinal behavioral assays, were done using a
21 linear mixed effect model to assess surgery (Sham/Injured), genotype (WT/VEGFA-null), weeks after
22 surgery (3/12), sex (M/F), and surgery (Naïve/Sham). Linear mixed effect models were initiated with
23 all factors and reduced in complexity as factors were found to be not significant. Additionally, focused
24 questions were modeled to assess injured groups with genotype and week. A 2 or 3 factor ANOVA was
25 used on terminal measures such as *Ex Vivo* CEμCT, biomechanics, disc degeneration scoring, or
26 immunohistochemistry to assess effects of injury, genotype, and sex. ANOVA pairwise comparisons
27 were done with the Fisher's Least Significant Difference method. Survival curves implemented Mantel-
28 Cox test while binary penetration results used a Fisher's exact test. Simple pairwise comparisons were
29 done using a Welch's t-test when appropriate. Appropriate adjustments were made in the respective
30 statistical models for unequal variances and non-normal distributions. The ROUT outlier test with
31 Q=0.1% removed definitive outliers within groups.[80] R and GraphPad Prism were used to model results.

For gene ontology analyses, biological pathways enriched by the upregulated and downregulated DEGs were identified by using the Panther Classification System with version Panther 19.0 by using the statistical overrepresentation test. For ECs, an adjusted p value of $p < 0.05$ and logFC of 0.41 was used to identify statistically significant DEGs with at least a 50% increase in fold change of the treatment group when compared to the control. For neuronal cells, an adjusted p value of $p < 0.10$ and logFC of 0.41 was used to identify statistically significant DEGs with at least a 50% increase in fold change of the treatment group when compared to the controls. The full list of all DEGs and GO terms for the endothelial cells comparisons are listed in Tables S8A and S8B and for the neuronal cell comparisons are listed in Tables S9A and S9B.

REFERENCES

1. Airaksinen O, Brox JI, Cedraschi C, et al. Chapter 4. European guidelines for the management of chronic nonspecific low back pain. *Eur Spine J*. Mar 2006;15 Suppl 2(Suppl 2):S192-300. doi:10.1007/s00586-006-1072-1
2. Hartvigsen J, Hancock MJ, Kongsted A, et al. What low back pain is and why we need to pay attention. *Lancet*. Jun 9 2018;391(10137):2356-2367. doi:10.1016/S0140-6736(18)30480-X
3. Yang H, Haldeman S. Behavior-Related Factors Associated With Low Back Pain in the US Adult Population. *Spine (Phila Pa 1976)*. Jan 1 2018;43(1):28-34. doi:10.1097/BRS.0000000000001665
4. Hoy D, March L, Brooks P, et al. The global burden of low back pain: estimates from the Global Burden of Disease 2010 study. *Ann Rheum Dis*. Jun 2014;73(6):968-74. doi:10.1136/annrheumdis-2013-204428
5. Shokri P, Zahmatyar M, Falah Tafti M, et al. Non-spinal low back pain: Global epidemiology, trends, and risk factors. *Health Sci Rep*. Sep 2023;6(9):e1533. doi:10.1002/hsr2.1533
6. Collaborators GBDLBP. Global, regional, and national burden of low back pain, 1990-2020, its attributable risk factors, and projections to 2050: a systematic analysis of the Global Burden of Disease Study 2021. *Lancet Rheumatol*. Jun 2023;5(6):e316-e329. doi:10.1016/S2665-9913(23)00098-X
7. Rannou F, Lee TS, Zhou RH, et al. Intervertebral disc degeneration: the role of the mitochondrial pathway in annulus fibrosus cell apoptosis induced by overload. *Am J Pathol*. Mar 2004;164(3):915-24. doi:10.1016/S0002-9440(10)63179-3
8. Feng Y, Egan B, Wang J. Genetic Factors in Intervertebral Disc Degeneration. *Genes Dis*. Sep 2016;3(3):178-185. doi:10.1016/j.gendis.2016.04.005
9. Wang F, Cai F, Shi R, Wang XH, Wu XT. Aging and age related stresses: a senescence mechanism of intervertebral disc degeneration. *Osteoarthritis Cartilage*. Mar 2016;24(3):398-408. doi:10.1016/j.joca.2015.09.019
10. Luoma K, Riihimäki H, Luukkonen R, Raininko R, Viikari-Juntura E, Lamminen A. Low Back Pain in Relation to Lumbar Disc Degeneration:. *Spine*. 02/2000 2000;25(4):487-492. doi:10.1097/00007632-200002150-00016
11. Urban JP. Swelling pressure of the lumbar intervertebral discs: influence of age, spinal level, composition, and degeneration. *Spine*. Feb 01 1988;13(2):179-187.
12. Buckwalter JA. Aging and degeneration of the human intervertebral disc. *Spine (Phila Pa 1976)*. Jun 1 1995;20(11):1307-14. doi:10.1097/00007632-199506000-00022
13. Adams MA, Freeman BJ, Morrison HP, Nelson IW, Dolan P. Mechanical initiation of intervertebral disc degeneration. *Spine (Phila Pa 1976)*. Jul 1 2000;25(13):1625-36. doi:10.1097/00007632-200007010-00005
14. Setton LA, Chen J. Mechanobiology of the intervertebral disc and relevance to disc degeneration. *The Journal of Bone and Joint Surgery American Volume*. 2006-04 2006;88 Suppl 2:52-57. doi:10.2106/JBJS.F.00001
15. Binch ALA, Fitzgerald JC, Growney EA, Barry F. Cell-based strategies for IVD repair: clinical progress and translational obstacles. *Nat Rev Rheumatol*. Mar 2021;17(3):158-175. doi:10.1038/s41584-020-00568-w
16. Binch ALA, Cole AA, Breakwell LM, et al. Nerves are more abundant than blood vessels in the degenerate human intervertebral disc. *Arthritis Research & Therapy*. 12/2015 2015;17(1)doi:10.1186/s13075-015-0889-6

17. Sato J, Inage K, Miyagi M, et al. Inhibiting Vascular Endothelial Growth Factor in Injured Intervertebral Discs Attenuates Pain-Related Neuropeptide Expression in Dorsal Root Ganglia in Rats. *Asian spine journal*. Aug 2017;11(4):556-561. doi:10.4184/asj.2017.11.4.556
18. Carmeliet P, Ruiz de Almodovar C. VEGF ligands and receptors: implications in neurodevelopment and neurodegeneration. *Cell Mol Life Sci*. May 2013;70(10):1763-78. doi:10.1007/s00018-013-1283-7
19. Falk T, Gonzalez RT, Sherman SJ. The yin and yang of VEGF and PEDF: multifaceted neurotrophic factors and their potential in the treatment of Parkinson's Disease. *Int J Mol Sci*. Aug 5 2010;11(8):2875-900. doi:10.3390/ijms11082875
20. Walk RE, Moon HJ, Tang SY, Gupta MC. Contrast-enhanced microCT evaluation of degeneration following partial and full width injuries to the mouse lumbar intervertebral disc. *Sci Rep*. Sep 16 2022;12(1):15555. doi:10.1038/s41598-022-19487-9
21. Leimer EM, Gayoso MG, Jing L, Tang SY, Gupta MC, Setton LA. Behavioral Compensations and Neuronal Remodeling in a Rodent Model of Chronic Intervertebral Disc Degeneration. *Sci Rep*. Mar 6 2019;9(1):3759. doi:10.1038/s41598-019-39657-6
22. Millecamps M, Stone LS. Delayed onset of persistent discogenic axial and radiating pain after a single-level lumbar intervertebral disc injury in mice. *PAIN®*. Sep 01 2018;159(9):1843. doi:10.1097/j.pain.0000000000001284
23. Rickman M, Ghim M, Pang K, et al. Disturbed flow increases endothelial inflammation and permeability via a Frizzled-4-beta-catenin-dependent pathway. *J Cell Sci*. Mar 15 2023;136(6)doi:10.1242/jcs.260449
24. Dejana E. The role of wnt signaling in physiological and pathological angiogenesis. *Circ Res*. Oct 15 2010;107(8):943-52. doi:10.1161/CIRCRESAHA.110.223750
25. Lohela M, Saaristo A, Veikkola T, Alitalo K. Lymphangiogenic growth factors, receptors and therapies. *Thromb Haemost*. Aug 2003;90(2):167-84. doi:10.1160/TH03-04-0200
26. Tammela T, Alitalo K. Lymphangiogenesis: Molecular mechanisms and future promise. *Cell*. Feb 19 2010;140(4):460-76. doi:10.1016/j.cell.2010.01.045
27. Cao R, Brakenhielm E, Li X, et al. Angiogenesis stimulated by PDGF-CC, a novel member in the PDGF family, involves activation of PDGFR-alphaalpha and -alphabeta receptors. *FASEB J*. Oct 2002;16(12):1575-83. doi:10.1096/fj.02-0319com
28. Page-McCaw A, Ewald AJ, Werb Z. Matrix metalloproteinases and the regulation of tissue remodelling. *Nat Rev Mol Cell Biol*. Mar 2007;8(3):221-33. doi:10.1038/nrm2125
29. Kessenbrock K, Plaks V, Werb Z. Matrix metalloproteinases: regulators of the tumor microenvironment. *Cell*. Apr 2 2010;141(1):52-67. doi:10.1016/j.cell.2010.03.015
30. Panopoulos AD, Watowich SS. Granulocyte colony-stimulating factor: molecular mechanisms of action during steady state and 'emergency' hematopoiesis. *Cytokine*. Jun 2008;42(3):277-88. doi:10.1016/j.cyto.2008.03.002
31. Hamilton JA. Colony-stimulating factors in inflammation and autoimmunity. *Nat Rev Immunol*. Jul 2008;8(7):533-44. doi:10.1038/nri2356
32. Zlotnik A, Yoshie O. The Chemokine Superfamily Revisited. *Immunity*. 05/2012 2012;36(5):705-716. doi:10.1016/j.immuni.2012.05.008
33. Appay V, Rowland-Jones SL. RANTES: a versatile and controversial chemokine. *Trends Immunol*. Feb 2001;22(2):83-7. doi:10.1016/s1471-4906(00)01812-3
34. Lee S, Millecamps M, Foster DZ, Stone LS. Long-term histological analysis of innervation and macrophage infiltration in a mouse model of intervertebral disc injury-induced low back pain. *J Orthop Res*. Jun 2020;38(6):1238-1247. doi:10.1002/jor.24560

35. Freemont AJ, Peacock TE, Goupille P, Hoyland JA, O apos Brien J, Jayson MI. Nerve ingrowth into diseased intervertebral disc in chronic back pain. *Lancet*. Jul 19 1997;350(9072):178-181. doi:10.1016/s0140-6736(97)02135-1
36. Brisby H. Pathology and possible mechanisms of nervous system response to disc degeneration. *J Bone Joint Surg Am*. Apr 2006;88 Suppl 2:68-71. doi:10.2106/JBJS.E.01282
37. Lama P, Le Maitre CL, Harding IJ, Dolan P, Adams MA. Nerves and blood vessels in degenerated intervertebral discs are confined to physically disrupted tissue. *J Anat*. Jul 2018;233(1):86-97. doi:10.1111/joa.12817
38. Krock E, Rosenzweig DH, Chabot-Dore AJ, et al. Painful, degenerating intervertebral discs up-regulate neurite sprouting and CGRP through nociceptive factors. *J Cell Mol Med*. Jun 2014;18(6):1213-25. doi:10.1111/jcmm.12268
39. Chen X, Chen Z, Ma G, et al. Reactive Oxygen Species Induced Upregulation of TRPV1 in Dorsal Root Ganglia Results in Low Back Pain in Rats. *J Inflamm Res*. 2024;17:2245-2256. doi:10.2147/JIR.S446841
40. Kameda T, Zvick J, Vuk M, et al. Expression and Activity of TRPA1 and TRPV1 in the Intervertebral Disc: Association with Inflammation and Matrix Remodeling. *Int J Mol Sci*. Apr 10 2019;20(7)doi:10.3390/ijms20071767
41. Shuba YM. Beyond Neuronal Heat Sensing: Diversity of TRPV1 Heat-Capsaicin Receptor-Channel Functions. *Front Cell Neurosci*. 2020;14:612480. doi:10.3389/fncel.2020.612480
42. Rosenbaum T, Simon SA. TRPV1 Receptors and Signal Transduction. In: Liedtke WB, Heller S, eds. *TRP Ion Channel Function in Sensory Transduction and Cellular Signaling Cascades*. 2007. *Frontiers in Neuroscience*.
43. Freemont AJ, Peacock TE, Goupille P, Hoyland JA, O'Brien J, Jayson MI. Nerve ingrowth into diseased intervertebral disc in chronic back pain. *Lancet*. Jul 19 1997;350(9072):178-81. doi:10.1016/s0140-6736(97)02135-1
44. Risbud MV, Shapiro IM. Role of cytokines in intervertebral disc degeneration: pain and disc content. Review. *Nature reviews Rheumatology*. Jan 2014;10(1):44-56. doi:10.1038/nrrheum.2013.160
45. Burke JG, Watson RWG, McCormack D, Dowling FE, Walsh MG, Fitzpatrick JM. Intervertebral discs which cause low back pain secrete high levels of proinflammatory mediators. *The Journal of bone and joint surgery British volume*. 2002;84(2):196-201.
46. Freemont AJ. The cellular pathobiology of the degenerate intervertebral disc and discogenic back pain. *Rheumatology (Oxford)*. Jan 2009;48(1):5-10. doi:10.1093/rheumatology/ken396
47. Grunhagen T, Wilde G, Soukane DM, Shirazi-Adl SA, Urban JPG. Nutrient Supply and Intervertebral Disc Metabolism. *Bone and Joint Surgery*. 2006 2006;88-A:30-35. doi:10.2106/JBJS.E.01290
48. Clayton SW, Walk RE, Mpofu L, Easson GWD, Tang SY. Sex-specific divergences in the types and timing of infiltrating immune cells during the intervertebral disc acute injury response and their associations with degeneration. *Osteoarthritis Cartilage*. Feb 2025;33(2):247-260. doi:10.1016/j.joca.2024.10.002
49. Johnson ZI, Schoepflin ZR, Choi H, Shapiro IM, Risbud MV. Disc in flames: Roles of TNF-alpha and IL-1beta in intervertebral disc degeneration. *Eur Cell Mater*. Sep 21 2015;30:104-16; discussion 116-7. doi:10.22203/ecm.v030a08
50. Millecamps M, Tajerian M, Naso L, Sage EH, Stone LS. Lumbar intervertebral disc degeneration associated with axial and radiating low back pain in ageing SPARC-null mice. *PAIN®*. Jun 2012;153(6):1167-1179. doi:10.1016/j.pain.2012.01.027

51. Oehme D, Goldschlager T, Ghosh P, Rosenfeld JV, Jenkin G. Cell-Based Therapies Used to Treat Lumbar Degenerative Disc Disease: A Systematic Review of Animal Studies and Human Clinical Trials. *Stem Cells Int*. 2015;2015:946031. doi:10.1155/2015/946031
52. Barbe MF, Chen FL, Loomis RH, et al. Characterization of pain-related behaviors in a rat model of acute-to-chronic low back pain: single vs. multi-level disc injury. *Front Pain Res (Lausanne)*. 2024;5:1394017. doi:10.3389/fpain.2024.1394017
53. Ruzankina Y, Pinzon-Guzman C, Asare A, et al. Deletion of the developmentally essential gene ATR in adult mice leads to age-related phenotypes and stem cell loss. *Cell Stem Cell*. Jun 7 2007;1(1):113-126. doi:10.1016/j.stem.2007.03.002
54. Gerber HP, Hillan KJ, Ryan AM, et al. VEGF is required for growth and survival in neonatal mice. *Development*. Mar 1999;126(6):1149-59. doi:10.1242/dev.126.6.1149
55. Madisen L, Zwingman TA, Sunkin SM, et al. A robust and high-throughput Cre reporting and characterization system for the whole mouse brain. *Nat Neurosci*. Jan 2010;13(1):133-40. doi:10.1038/nn.2467
56. Liu JW, Lin KH, Weber C, et al. An In Vitro Organ Culture Model of the Murine Intervertebral Disc. *Journal of visualized experiments : JoVE*. Apr 11 2017;(122):e55437-e55437. doi:10.3791/55437
57. Andersson GB. Epidemiological features of chronic low-back pain. *Lancet*. Aug 14 1999;354(9178):581-5. doi:10.1016/S0140-6736(99)01312-4
58. Atlas SJ, Deyo RA. Evaluating and managing acute low back pain in the primary care setting. *J Gen Intern Med*. Feb 2001;16(2):120-31. doi:10.1111/j.1525-1497.2001.91141.x
59. Melgoza IP, Chenna SS, Tessier S, et al. Development of a standardized histopathology scoring system using machine learning algorithms for intervertebral disc degeneration in the mouse model-An ORS spine section initiative. *JOR Spine*. Jun 2021;4(2):e1164. doi:10.1002/jsp2.1164
60. Scheller E, Brazill JM, Lorenz M. Spatial mapping and contextualization of axon subtypes innervating the long bones of C3H and B6 mice. protocolsio2021.
61. Hodgdon KE, Hingtgen CM, Nicol GD. Dorsal root ganglia isolated from Nf1+/- mice exhibit increased levels of mRNA expression of voltage-dependent sodium channels. *Neuroscience*. Mar 29 2012;206:237-44. doi:10.1016/j.neuroscience.2011.12.045
62. Roza C, Laird JM, Souslova V, Wood JN, Cervero F. The tetrodotoxin-resistant Na+ channel Nav1.8 is essential for the expression of spontaneous activity in damaged sensory axons of mice. *J Physiol*. Aug 1 2003;550(Pt 3):921-6. doi:10.1113/jphysiol.2003.046110
63. Bird EV, Christmas CR, Loescher AR, et al. Correlation of Nav1.8 and Nav1.9 sodium channel expression with neuropathic pain in human subjects with lingual nerve neuromas. *Mol Pain*. Oct 21 2013;9:52. doi:10.1186/1744-8069-9-52
64. Walk RE, Tang SY. In vivo contrast-enhanced microCT for the monitoring of mouse thoracic, lumbar, and coccygeal intervertebral discs. *JOR Spine*. Jun 01 2019;2(2)doi:10.1002/jsp2.1058
65. Lin KH, Wu Q, Leib D, Tang SY. A Novel Technique for the Contrast-Enhanced microCT Imaging of Murine Intervertebral Discs. *Journal of the mechanical behavior of biomedical materials*. Jun 2016;doi:10.1016/j.jmbbm.2016.06.003
66. Easson GWD, Savadipour A, Anandarajah A, et al. Modulation of TRPV4 protects against degeneration induced by sustained loading and promotes matrix synthesis in the intervertebral disc. *FASEB J*. Feb 2023;37(2):e22714. doi:10.1096/fj.202201388R
67. Goh J, Ladiges W. Voluntary Wheel Running in Mice. *Curr Protoc Mouse Biol*. Dec 2 2015;5(4):283-290. doi:10.1002/9780470942390.mo140295

68. Chaplan SR, Bach FW, Pogrel JW, Chung JM, Yaksh TL. Quantitative assessment of tactile allodynia in the rat paw. *J Neurosci Methods*. Jul 1994;53(1):55-63. doi:10.1016/0165-0270(94)90144-9
69. Sheahan TD, Siuda ER, Bruchas MR, et al. Inflammation and nerve injury minimally affect mouse voluntary behaviors proposed as indicators of pain. *Neurobiol Pain*. Aug-Dec 2017;2:1-12. doi:10.1016/j.ynpai.2017.09.001
70. Duraku LS, Hossaini M, Hoendervangers S, et al. Spatiotemporal dynamics of re-innervation and hyperinnervation patterns by uninjured CGRP fibers in the rat foot sole epidermis after nerve injury. *Mol Pain*. Aug 30 2012;8:61. doi:10.1186/1744-8069-8-61
71. Allen KD, Griffin TM, Rodriguiz RM, et al. Decreased physical function and increased pain sensitivity in mice deficient for type IX collagen. *Arthritis Rheum*. Sep 2009;60(9):2684-93. doi:10.1002/art.24783
72. Kamisli S, Karakurt A, Uyumlu AB, et al. Evaluation of the effects of novel nafimidone derivatives on thermal hypoalgesia in mice with diabetic neuropathy. *Balkan Med J*. Mar 2013;30(1):94-8. doi:10.5152/balkanmedj.2012.067
73. Samineni VK, Yoon J, Crawford KE, et al. Fully implantable, battery-free wireless optoelectronic devices for spinal optogenetics. *Pain*. Nov 2017;158(11):2108-2116. doi:10.1097/j.pain.0000000000000968
74. Jain S, Golden JP, Wozniak D, Pehek E, Johnson EM, Jr., Milbrandt J. RET is dispensable for maintenance of midbrain dopaminergic neurons in adult mice. *J Neurosci*. Oct 25 2006;26(43):11230-8. doi:10.1523/JNEUROSCI.1876-06.2006
75. Deacon RM. Measuring the strength of mice. *J Vis Exp*. Jun 2 2013;(76)doi:10.3791/2610
76. Meyer OA, Tilson HA, Byrd WC, Riley MT. A method for the routine assessment of fore- and hindlimb grip strength of rats and mice. *Neurobehav Toxicol*. Fall 1979;1(3):233-6.
77. Barcellona MN, Speer JE, Fearing BV, et al. Control of adhesive ligand density for modulation of nucleus pulposus cell phenotype. *Biomaterials*. Aug 2020;250:120057. doi:10.1016/j.biomaterials.2020.120057
78. Bridgen DT, Fearing BV, Jing L, et al. Regulation of human nucleus pulposus cells by peptide-coupled substrates. *Acta Biomater*. Jun 2017;55:100-108. doi:10.1016/j.actbio.2017.04.019
79. Moon HJ, Yurube T, Lozito TP, et al. Effects of secreted factors in culture medium of annulus fibrosus cells on microvascular endothelial cells: elucidating the possible pathomechanisms of matrix degradation and nerve in-growth in disc degeneration. *Osteoarthritis and Cartilage*. 02/2014 2014;22(2):344-354. doi:10.1016/j.joca.2013.12.008
80. RE MHaB. Detecting outliers when fitting data with nonlinear regression – a new method based on robust nonlinear regression and the false discovery rate. *BMC Bioinformatics*. 2006;7(123)

List of Abbreviations

AF – Annulus Fibrosus
Ai9 – Cre-reporter expressing tdTomato fluorescent protein (Rosa-CAG-LSL-tdTomato)
ANOVA – Analysis of Variance
CEμCT – Contrast-Enhanced Micro-Computed Tomography
CLBP – Chronic Low Back Pain
CM – Conditioned Media
CTCF – Corrected Total Cell Fluorescence
C57BL/6J – Common inbred mouse strain
DAPI – 4′,6-Diamidino-2-Phenylindole (DNA stain)
DEG – Differentially Expressed Gene
DHI – Disc Height Index
DRG – Dorsal Root Ganglion
EC – Endothelial Cell (HMEC-1)
EDTA – Ethylenediaminetetraacetic Acid (chelating agent)
ELISA – Enzyme-Linked Immunosorbent Assay
EMCN – Endomucin (endothelial cell marker)
EMEM, ATCC – Eagle's Minimum Essential Medium, from American Type Culture Collection
ERT2 – Modified Estrogen Receptor Ligand Binding Domain (used in tamoxifen-inducible Cre systems)
EVF – Electronic Von Frey
FBS – Fetal Bovine Serum
FITC – Fluorescein Isothiocyanate dye
FSU – Functional Spinal Unit
HBSS – Hanks' Balanced Salt Solution
HMEC-1 – Human Microvascular Endothelial Cell Line
IL1β – Interleukin 1 Beta
IVD – Intervertebral Disc
LBP – Low Back Pain
LoxP – Locus of X-over P1 (recombination sites for Cre-Lox systems)
LSD – Least Significant Difference (statistical post hoc test)
MCDB – Molecular, Cell, and Developmental Biology
Nav1.8 – Voltage-Gated Sodium Channel (gene SCN10A) expressed in nociceptive neurons
NC – Neuron cells (SH-SY5Y)
NFkB – Nuclear Factor Kappa B
NGF – Nerve Growth Factor
NI/DI – Nucleus Attenuation Intensity/Disc Attenuation Intensity
NP – Nucleus Pulposus
OCT – Optimal Cutting Temperature Compound
PAP – Hydrophobic barrier pen
PBS – Phosphate-Buffered Saline
PGP9.5 – Protein Gene Product 9.5 (neuronal marker)
P/S – Penicillin/Streptomycin
ROI – Region of Interest
SCRAM – Scrambled siRNA (negative control)
SH-SY5Y – Human Neuroblastoma Cell Line
siRNA – Small Interfering RNA
SNT – Simple Neurite Tracer (ImageJ plugin)
TNFα – Tumor Necrosis Factor Alpha
TNT – Tris-NaCl-Tween buffer
TrKA – Tropomyosin Receptor Kinase A (NGF receptor)
TRPA1 – Transient Receptor Potential Ankyrin 1
TRPV1 – Transient Receptor Potential Vanilloid 1
UBC – Ubiquitin
VEGF – Vascular Endothelial Growth Factor
WT – Wild Type

Acknowledgments:

We acknowledge the support of the Washington University Musculoskeletal Research Center Structure and Function Core (Michael Brodt); Histology Core (Crystal Idleburg and Samantha Coleman); and Animal Behavior and Function Core. We also acknowledge Kelsey Collins and Washington University Pain Center Judith Golden for their training in behavioral assessments of pain. We thank Jenny McKensie and Evan Buettmann for assistance in working with the VEGFA-null animals. We thank the Washington University Genomics Technology Access Core (GTAC), and the Eve-tech for the multiplex ELISA analysis.

Funding:

This work was conducted with funding support from National Institute of Health:

National Institutes of Health grant R21AR081517 (ST/MG)

National Institutes of Health grant R01AR074441 (ST)

National Institutes of Health grant R01AR077678 (LS/ST)

National Institutes of Health grant P30AR074992 (MS)

National Institutes of Health grant S10OD028573 (MS)

Author contributions:

Conceptualization: RSP, SYT

Methodology: RSP, REW, HJM, ALL, ANS, SWC, LJ, LAS, MCG, SYT

Data Interpretation: Methodology: RSP, REW, HJM, ALL, ANS, SWC, LJ, LAS, MCG, SYT

Investigation: RSP, HJM, ALL, LJ, LAS, MCG, SYT

Visualization: RSP, HJM, ALL, SWC

Funding acquisition: LAS, MCG, SYT

Project administration: RSP

Supervision: SYT

Writing – original draft: RSP, HJM, ALL

Writing – review & editing: RSP, SWC, SYT

Competing interests:

Provisional Patent: 020859/US

Title: VEGFA INHIBITORS AS A TREATMENT FOR CHRONIC MECHANICAL ALLODYNIA

Co-inventors: RSP, HJM, MCG, SYT

Data and materials availability: All data, code, and materials used in the analysis must be available in some form to any researcher for purposes of reproducing or extending the analysis. Include a note explaining any restrictions on materials, such as materials transfer agreements (MTAs). Note accession numbers to any data relating to the paper and deposited in a public database; include a brief description of the data set or model with the number. If all data are in the paper and supplementary materials, include the sentence